Structural, Transport and Magnetic Properties of Double Exchange $(Fe_{1-x}Mn_x)_{75}P_{15}C_{10}$ Amorphous Ferromagnetic Alloys

by

Md. Kamruzzaman

Roll No. 100614018F

Session: October-2006

A dissertation submitted in partial fulfillment of the requirement for the degree of M.Phil. in the Department of Physics, Bangladesh University of Engineering and Technology, Dhaka-1000

Department of Physics
BANGLADESH UNIVERSITY OF ENGINEERING AND TECHNOLOGY
Dhaka-1000, Bangladesh
April- 2010

BANGLADESH UNIVERSITY OF ENGINEERING AND TECHNOLOGY

DEPARTMENT OF PHYSICS, DHAKA-1000

Certification of thesis work

The thesis titled **"Structural, Transport and Magnetic Properties of Double Exchange $(Fe_{1-x}Mn_x)_{75}P_{15}C_{10}$ Amorphous Ferromagnetic Alloys",** submitted by Md. Kamruzzaman, Roll No.: 100614018F, Session-October- 2006, has been accepted as satisfactory in partial fulfillment of the requirement for the degree of Master of Philosophy (M. Phil.) in Physics on 17 April, 2010.

BOARD OF EXAMINERS

1. _____
   Dr. Md Feroz Alam Khan — Supervisor
   Professor, Department of Physics
   BUET, Dhaka-1000

2. _____
   Dr. A.K.M. Akther Hossain — Chairman
   Professor, Department of Physics
   BUET, Dhaka-1000

3. _____
   Dr. Md. Abu Hashan Bhuiyan — Member
   Professor, Department of Physics
   BUET, Dhaka-1000

4. _____
   Dr.Khondkar Siddique-e Rabbani — Member (External)
   Professor, Department of Biomedical Physics & Technology
   University of Dhaka, Dhaka-1000

Dedicated to

My Parents

Candidate's Declaration

It is hereby declared that this thesis or any part of it has not been submitted elsewhere for the award of any degree or diploma.

(Signature of the Candidate)

Md. Kamruzzaman

(Name of the Candidate)

Acknowledgements

All of my acknowledgements and gratitude to the almighty Allah for the successful completion of this dissertation.

It is my pleasure to express the perpetual indebtedness to my research supervisor **Dr. Md. Feroz Alam Khan**, Professor, Department of Physics, Bangladesh University of Engineering and Technology, Dhaka, for his supervision, constant guidance, untold patience, valuable suggestions and inspiration which allowed me to complete this thesis work.

I would like to express my sincere thanks to Professor Dr. A.K.M Akther Hossain, Head, Department of Physics, BUET for valuable suggestions and inspiration to complete the dissertation.

I would like to thank to all other teachers of the department of Physics, BUET specially Professor Dr. Nazma Zaman, Professor Dr. Md. Abu Hashan Bhuiyan, Professor Dr. Jiban Poddar, Professor Dr. Md. Mostak Hossain, Dr. Afia Begum, Dr. Forhad Mina, Mr. Rakibul Islam, Abu Sayem Karal, Muhammad Samir Ullah, Md. Jellur Rahman, for their encouragement and help during my research work.

I would like to thank Dr. Md. Abdul Gafur, Sr. Engineer, PP & PDC and Mr. Jasim Uddin Khan, Scientific Officer, BCSIR, Dhaka. I would like to thank Dr. D.K. Shah and Md. Nazrul Islam Khan BAED, for their invaluable contributions on this research work. I would also like to thank Mr. Rama Bijoy Sarker and Mr. Sunirmal Mojumder PhD researcher for valuable suggestions and discussion during my research work.

I am very grateful to my sister Ms.Tamjida Rahman Luna, Assistant Professor (OSD), Directorate of Secondary and Higher Secondary Education, Dhaka, and Mr. Kamal Uddin Azad, lecturer, Directorate of Secondary and Higher Secondary Education, Dhaka.

I am thankful to Mr. Md. Idris Munsi, Assistant Technical Officer of the Department of Physics for his sincere help and cooperation during the thesis work.I express my sincere thanks to the M.Phil researchers, Tahamida, Kollol, Binindita, Ranojit, Babu, for their friendly attitude. I also would like to thank to other M.Phil students of the Department of Physics for their kind help and inspirations. Thanks are given also to all staff members of the Department of Physics, BUET for giving support to my research work.

I would also like to express my gratefulness to the authority of BUET for giving me the opportunity to do this research work and financial support.

I am thankful to the International Program in Physical Science (IPPS) for providing expensive instruments to the Department of Physics , BUET which are used in this work.

Finally, I would like to express my heartfelt gratitude to my Parents and other family members for their constant support and encouragement during this research work.

CONTENTS

CHAPTER-4: EXPERIMENTAL TECHNIQUES

CHAPTER-5: RESULTS AND DISCUSSION

CHAPTER-6: CONCLUSIONS AND FUTURE WORK

LIST OF FIGURES

Chapter-2

Chapter-3

Chapter-4

Chapter-5

LIST OF TABLES

ABSTRACT

$(Fe_{1-x}Mn_x)_{75}P_{15}C_{10}$ (x=0.0, 0.10, 0.20 and 0.30) alloys have been prepared in the form of ribbon by standard melt-spinning technique in air with wheel speed of 25 m/sec and cooling rate $1.8x10^6$ K/sec. The prepared samples have been characterized by the structural, transport and magnetic properties measurements. The structural property of the alloys is confirmed by an X-ray diffraction experiment. X-ray diffraction patterns confirm the amorphous nature of the samples. The transport property is carried out at room temperature and the temperature range (93-298)K. Room temperature resistivity increases with the increase of Mn in the system. The magnetic impurities, scattering and topological spin disorder are thought to be responsible for the increase of resistivity of the samples. Normalized resistivity increases slightly with decrease in temperature for samples x=0.10 and x=0.20 and decreases with the decrease in temperature for samples x=0.00, 0.30. But for x=0.30, normalized resistivity gradually decreases upto 137K afterwards the resistivity increases with the decrease in temperature. This behavior is assumed to have been originated from the structural and topological scattering contribution. The magnetoresistance of the samples varied from 0 to 6% upto 0.57T applied magnetic field. Room temperature Hall resistivity measurement shows that the anomalous Hall effect which is attributed to the anisotropic spin scattering centers, magnons and the magnetic impurities.

DTA measurement shows that an exothermic peak arises above 690 K for each sample which indicates the onset of crystallization of the grains. TGA measurement shows that mass is slightly gained in all samples.

The real permeability decreases with the increase of Mn content and also with the frequency. Imaginary permeability increases linearly with the frequency which means that at higher frequency domains do not follow the applied force.

Magnetization measurement shows that saturation magnetization and the average magnetic moment per formula unit of $(Fe_{1-x}Mn_x)_{75}P_{15}C_{10}$ decreases with the increase of Mn content.

Chapter-1

Introduction

1.1 Introduction

An amorphous metal is a metallic material with a disordered atomic-scale structure. In contrast to most metals, which are crystalline and therefore have a highly ordered arrangement of atoms. Amorphous alloys are non-crystalline materials in which disordered structure is produced directly from the liquid state during cooling are called "glasses", and so amorphous metals are commonly referred to as "metallic glasses" or "glassy metals". The first reported metallic glass was an alloy $Au_{75}Si_{25}$ produced at Caltech by W. Klement, Willens and Duwez in 1960 [1]. This and other early glass-forming alloys had to be cooled rapidly to avoid crystallization. An important consequence of this was that metallic glasses could only be produced in a limited number of forms typically ribbons, foils, or wires in which one dimension was small so that heat could be extracted quickly enough to achieve the necessary cooling rate. As a result, metallic glass specimens were limited to thicknesses of less than one hundred micrometers. In 1976, H. Liebermann and C. Graham developed a new method of manufacturing thin ribbons of amorphous metal on a super cooled fast-spinning wheel [2]. This was an alloy of iron, nickel, phosphorus and boron. In the early 1980s, glassy ingots with 5 mm diameter were produced from the alloy of $Pd_{55}Pb_{22.5}Sb_{22.5}$ by surface etching followed with heating-cooling cycles. Using boron oxide flux, the achievable thickness was increased to a centimeter. Metallic glasses have been found to be promising for technological applications. It is discovered by Yoshizawa *et al* [3] [in 1988. There are two technologically important classes of magnetic amorphous alloys; the transition metal-metalloid (TM-M) alloys and the rare earth-transition metal (RE-TM) alloys. The TM-M alloys typically contain about 80 atom % Fe, Co, or Ni with the remainder being B, C, Si, P or Al as glass forming materials. The presence of the metalloids is necessary to lower the melting point, making it possible to quench the alloy through its glass temperature rapidly enough to form the amorphous phase. The present study involves the preparation of Fe based

amorphous ribbons. In this amorphous ribbons P and C have been used as glass forming materials. Here the Fe have been partially replaced by Mn, the general composition being $(Fe_{1-x}Mn_x)_{75}P_{15}C_{10}$ [x=0.00, 0.10, 0.20 and 0.30].

The melt-spinning technique has been used for the preparation of $(Fe_{1-x}Mn_x)_{75}P_{15}C_{10}$ [x=0.00, 0.10, 0.20 and 0.30] ribbons. The methods of the preparation of the ribbons are described in chapter-2 along with the procedure and conditions for glass forming amorphous materials.

The structural property studies of the materials are most important for the explanation of behavior of that material due to engineering and scientific applications. The studies of the magnetic properties of amorphous ribbons are significant for a variety of applications such as power generator transformers, magnetic heads, magnetic shielding etc. These applications may be determined by static (dc) or dynamic (ac) properties of the amorphous system.

Moreover, the temperature dependence and the stability and cost of materials are to be considered besides their magnetic properties. The dc and ac properties provided characteristics suitable for different types of applications. Generally high electrical resistivity, high mechanical strength, good corrosion resistance, and absence of crystalline anisotropy, structural defects and grain boundaries characterize amorphous ribbons. The magnetic properties such as saturation flux density, Curie temperature, magnetostriction and induced anisotropy can be controlled by the alloy composition and a subsequent heat treatment. The high electrical resistivity and the small thickness of the melt-quenched ribbons lead to low eddy current losses. The low hysteresis losses, results in very low core losses, which is of interest for power electronics at high frequencies. For application in small electronic devices, the amorphous ribbons have somewhat poorer losses than the conventional Fe-Ni-B ribbon. The design optimization requires lower cost of amorphous ribbons, higher induction compared to Fe-Ni-B ribbons. Amorphous ribbons have many refined applications also like development of magnetic bubbles for computer memory, amorphous superconductors etc. Research in the theoretical understanding, development and application of amorphous ribbons can thus be profitable, especially at its present new phase.

1.2 Aim of this Work

Amorphous ferromagnetism has been a subject of considerable interest in recent years [4].Both experimental and theoretical progress have been made towards a better understanding of the ferromagnetic ordering in solids which do not possess long-range periodicity in the atomic arrangement. In recent years, metallic glasses have received considerable experimental and theoretical attention owing to their anomalous magnetotransport and soft magnetic properties. These materials are interesting from both the fundamental and applied viewpoints. Because of various superior mechanical, magnetic and electrical properties, in comparison with those of the crystalline state, metallic glasses form a class of technologically important materials. They have already been put into applications in the devices e.g., choke coils, high frequency transformers and the magnetic thin film heads, reported in 1991 by Yoshizawa et al [5].

.

The objective of this work is to study structural, temperature and field dependence electrical resistivity, magnetoresistance, Hall resistivity, thermal property, magnetization and frequency dependent complex permeability of $(Fe_{1-x}Mn_x)_{75}P_{15}C_{10}$ magnetic alloys, and the effect of manganese (Mn) there on. The studies involved in the present work would provide useful information about its potentials in high frequency switching, spin wave devices and sensor devices as well as low and high temperature power applications. In order to achieve the aforesaid objective, the following main steps are included in the present work:

(1) X- ray diffraction analysis
(2) The *I~V* measurement for resistivity and magnetoresistance in different magnetic fields that ranges form 0 to 0.57T at room temperature, low temperature, range: (93- 298)K
(3) Hall coefficient and Hall resistivity in the range 0-0.57T magnetic field at room temperature.
(4) Magnetization measurement at room temperature

(5) The measurement of Differential Thermal Analysis (DTA), Thermo Gravimetric Analysis (TGA) and Differential Thermo Gravimetric (DTG) Analysis for the investigation of thermal response of the ribbons

(6) The measurement of permeability at room temperature in the low frequency range (100Hz- 100 MHz)

1.3 Review of the Previous Work

The main intrinsic properties of metallic glasses so far investigated are the ferromagnetic Curie temperature (T_C), and Mössbauer study. As the extrinsic properties, coercive force, remenance to saturation magnetic ratio has been studied. Another important field of study on metallic glass system is to investigate the transport and magneto transport properties.

Transport and magnetic properties of amorphous $(Fe_{1-x}Mn_x)_{75}P_{15}C_{10}$ alloys have been studied with x=0.05 and x= 0.5 by Heinemann K. and Barner K.[6], found zero coercive field $H_{c;}$ for x=0.05 and upper limit $H_c \leq 1.5$G, the crystallization temperatures T_{cr}=740 K (x=0.5) and T_{cr}=710 K (x=0.05), resistivity of the order of 10^{-6} Ω-m, Curie temperature T_c is 552 K, magnetic moment per cation is 0.42 μ_B.

Thermoelectric Power of some $(Fe_{1-x}\ Mn_{\ x})_{75}P_{15}C_{10}$ amorphous Alloys (x=0, 0.05, 0.20, 0.30) were studied my Kraus E. *et. al.*[7]. Variation of x from 0 to 1 changes the magnetic transition from an amorphous ferromagnetic $Fe_{75}P_{15}C_{10}$ to an amorphous antiferromagnetic $Mn_{75}P_{15}C_{10}$ [8,9].

Pressure derivative of T_c in amorphous $(Fe_{100-x}Mn_x)_{75}P_{15}C_{10}$ alloys with x = 0, 5, 10, 20, 30 have been investigated by Medvedeva I.V. *et. al.*[10]. They showed that the Curie temperature T_c decreases with pressure.

References

1. Klement, J.W., Willens, R.H. and Duwez, P., "Non-crystalline structure in solidified gold-silicon alloys", Nature 187 p 869 – 870 (1960)

2. Libermann, H., and Graham, C., "Production Of Amorphous Alloy Ribbons And Effects Of Apparatus Parameters On Ribbon Dimensions" , IEEE Transactions on Magnetics, Vol Mag-12, No 6 (1976)

3. Yoshizawa, Y., Oguma, S. and Yamauchi, K., "New Fe-Based Soft Magnetic Alloys Composed of Ultrafine Grain Structure", J. Appl. Phys. 64, 6044–6046 (1988)

4. Amophous Magnetism, edited by H.O. Hopper and A.M deGraaf (Plenum, New York , 1973)

5. Yoshizawa, Y. and Yamauchi, K., "Magnetic properties of Fe-Cu-M-Si-B (M = Cr, V,. Mo, Nb, Ta, W) alloys", Mater Sci. Eng. A 133 p176-179 (1991)

6. Heinemann, K. and Barner, K., "Transport and magnetic properties of amorphous $(Fe_{1-x}Mn_x)_{75}P_{15}C_{10}$ alloys", J.Magn. Magn. Mater. 42 p291-294 (1984)

7. Kraus, E., Heinemann, K., Barner, K., Khan, F.A., Medvedeva I.V., Schicketanz H.,and Terzieff, "Thermoelectric Power of some $(Fe_{1-x}Mn_x)_{75}P_{15}C_{10}$ amorphous Alloys", Phys. Stal. Sol. (a) 177 p547 (2000)

8. Sinha, A.K., "Magnetic transition from an amorphous ferromagnetic $Fe_{75}P_{15}C_{10}$ to an amorphous antiferromagnetic $Mn_{75}P_{15}C_{10}$", J. Appl. Phys. 42 p338 (1971)

9. Hasegawa, R., "Magnetic Properties of an Amorphous Mn-P-C Alloy" Phys. Rev. B3, p1631 (1971)

10. Medvedeva, I.V., Bersenev, Yu.S., Ganin A.A., Barner K., Schunemann J.W. and Heinemann K., "Pressure derivative of T_c in amorphous $(Fe_{100-x}Mn_x)_{75}P_{15}C_{10}$ alloys", J. Magn. Magn. Mater. 124 p293 (1993)

Chapter-2

Preparation of Amorphous Ribbons

2.1 Introduction

Amorphous solid glass which has no precise meaning, it believed from the long time that amorphous system could not exist ferromagnetism. There are different methods produced to prepare the amorphous ribbons. This trend abolishes after the discovery of metallic glass by Klement, J.W et. al.[1] and Gobonov in the same time. There argument was based on the evidence that the electronic band structure of crystalline solids did not changes in any fundamental way on transition on the liquid state. A real technological interest developed after Pond, R. Jr and Maddin, R [2] reported on the preparation of continuous ribbons of amorphous alloys.

The technological interest developed after Pond, R. Jr and Maddin, R [2] reported on the preparation of continuous ribbons of amorphous alloys. The theoretically expected retention of ferromagnetic behavior in amorphous solids was first demonstrated by Marder and Nowick in their work on vacuum deposited Co-Au alloys and soon there after by Tsuei and Duwez [3] in their work on split-cooled Pd-20at% Si containing some ferromagnetic element partially substituted for the Pd.

The positive ways to have the amorphous state of pure metal like Fe, Ni, Co etc at low temperature. Alloys of these metals with glass forming materials can be obtained in the amorphous state by cooling the melt at least a million degrees per second which can remain in the metastable state over an extended range of temperature.

Two important classes of amorphous magnetic materials are being studied intensively in recent time. They are the transition metal-metalloid (TM-M) glass and the rare-earth transition metal glass (RE-TM) reported by R. Alben et. al.[4] and G. S. Cargil III [5]. TM-M glasses are stable for composition around 75-80% of TM (Fe, Co, Ni etc. or in their combinations) and 25-20% of the metalloid (P, C, Si, B or Al in their combinations). Typical composition for RE-TM glass is RE33-TM67 where RE is one of the rare-earth metals like Gd, Tb, Dy, Y etc. and TM is one of the 3d transition metals like Fe, Co or Ni. Recently the metalloids in

TM-M glass is replaced by non-magnetic metals like Zr, Hf, etc. by T. Masumoto et. al.[6]. The new amorphous and metastable alloys prepared by such techniques were used in the early works to explore the many possibilities opened up by these new rapid quenching techniques.

2.2 Conditions for glass formation of amorphous materials

In terms of viscosity and diffusion co-efficient we can find the conditions for formation glass.

(a) In metals atomic bonding is metallic and viscosity is low and the diffusion co-efficient and mobility is high.

(b) In the case of amorphous material viscosity is very high and the mobility and the diffusion co-efficient are low. Atomic bonds tend to be covalent as in the case of silicate (SiO_2)

2.3 Preparation technique of amorphous ribbon

There are various techniques is used to produce a metallic alloy in an amorphous state where the atomic arrangements have no long-range periodicity. The different experimental techniques developed to produce amorphous metallic glass can be classified into two groups.

(a) The atomic deposition methods and

(b) The fast cooling of the melt

2.3.1 The atomic deposition methods

Deposition can be described in terms of whether the added atom is prevented from diffusing more than an atomic distance before it is fixed in position due to cooling and increased viscosity. The atomic deposition methods include condensation of a vapor on a cooled substrate by

(i) Vapor deposition

(ii) Sputtering deposition

(iii) Electro deposition

(iv) Chemical deposition

2.3.2 The fast cooling of the melt

For producing of an amorphous state by any of the liquid quenching devices, the alloy must be cooled through the temperature range from the melting temperature (T_m) to the glass transition temperature (T_g) very fast allowing no time for crystallization. The factors controlling T_g and crystallization are both structural and kinetic. The structural factors are concerned with atomic arrangement, bonding and atomic size effects. The kinetic factors as discussed by Turnbull [7] are the nucleation, crystal growth rate and diffusion rate compared to the cooling rate. The interest in this method stems from the wide variety of alloys that can be made as well as from the potential low cost of preparation. In the pioneering work of Duwez et. al. [8], a number of devices has been reported for obtaining the necessary high quenching rates and for producing continuous filaments. The methods using the principle of fast cooling of melt techniques are:

(i) The gun technique
(ii) The melt spinning technique
(iii) Double roller rapid quenching technique
(iv) Centrifuge and rotary split quenching technique
(v) Torsion catapult technique
(vi) Plasma-jet spray technique
(vii) Filamentary casting technique
(viii) Melt extraction technique
(ix) Free jet spinning technique

Although the different methods used in preparing amorphous metallic ribbons are mentioned here, only the melt spinning technique which was used to prepare the specimens for the present work will be discussed.

2.3.2.1 The Melt Spinning Technique

The metallic glasses are prepared by several methods employing special techniques which involve rapid solidification of the melt. Melt spinning is one such technique used to prepare metallic glasses. In order to prepare $(Fe_{1-x}Mn_x)_{75}P_{15}C_{10}$ metallic glasses, the required quantity of metal-metal or metal-metalloid alloys are

taken in a quartz tube in their stoichiometric ratio wt%. A set of heater coils surround the quartz tube at one end and the temperature of the heater coil is kept more than the melting point of the alloy compound. Therefore, the melt of the alloy compound is formed at one end of the quartz tube. The melt is kept above the melting point of alloy until a homogeneous mixing in obtained. An inert gas is flows through the other end of the quartz tube after the homogeneous mixing is formed. The molten alloy flow through the outlet of the quartz tube and it is cooled at an ultra-fast rate with the help of a rotating cooled copper cylinder. On impact with the rotation drum, the melt is frozen within a few milli-second producing a long ribbon of metallic glasses. The experimental set up used for the above process is shown in Fig- 2.1

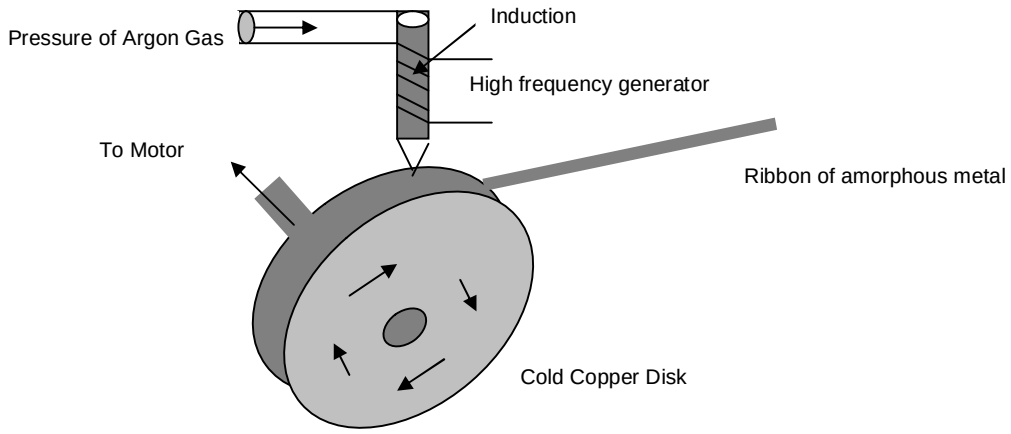

Figure 2.1: The experimental set up used for the melt spinning technique

2.4 Experimental details for the preparation of amorphous ribbon

The metallic glass ribbons are usually prepared in a furnace with an argon atmosphere (0.2 to 0.3 atmps.). The buttons prepared are of about 50 grams each. Care is taken to ensure thorough mixing and homogeneity of the alloy composition, by turning over and re-melting each button few times. The mother alloys, formed in the form of buttons in a furnace by sudden cooling, are then cut into small pieces and is inserted in the quartz tube. The quartz tube is connected from the top by rubber 'O' rings and metal rings to the argon cylinder through a valve and a pressure gauge. After proper cleaning of the roller surface and adjusting its speed to the desired value, as measured

by stroboscope, the induction furnace is powered using high frequency generator. When the melting temperature is reached as observed through a protective spectacle, the injection pressure is applied by opening the pressure valve. To avoid the turbulence of the wind, arising from the high-speed roller in distributing the melt puddle, cotton pad and metallic shield are usually used just beneath the roller. To avoid oxidation of the ribbon during its formation, an inert atmosphere is created around the roller by a slow stream of helium gas. The speed of the roller, the volumetric flow rate, the orifice diameter, the substrate orifice distance, the injection angle etc. are adjusted by trial and error to get the best result in respect of the quality and the geometry of the ribbons. Important factors to control the thickness of ribbons are as follows

(a) Angular velocity, ω~2000 rev/min.

(b) Surface velocity, v ~ 25 m/s

(i) Gap between the nozzle and rotating copper drum is ~ 100 to 150 μm.

(ii) Oscillations of the rotating copper drum both static and dynamic have maximum displacement of ~ 1.5 μm

(iii) Pressure = 0.2 to 0.3 argon atmosphere.

(iv) Temperature of the metal Tm ≈ 1500°C. The temperature should not exceed 1800° C otherwise quartz tube would melt.

(v) Stability is ensured for the drop to fall on the surface of the spinning drum

2.5 Factors contributing to glass formation

There are three interrelated factors that determine glass-forming tendency. These are thermodynamic conditions that favor the liquid phase relative to the crystalline phase, the kinetic conditions that inhibit crystallization and the process factors that arise due to experimental conditions.

The thermodynamic factors for glass formation are liquids temperature T_m at which the alloy melts, the heat of vaporization and the free energy of all the phases that arise or could potentially arise during solidification process. Viscosity of the melt, the glass transition temperature T_g and the homogeneous nucleation rate belongs to kinetic parameters. The glass transition temperature is defined as the temperature at which

the super cooled liquid takes on the rigidity of a solid of more specifically at which the viscosity approached 15 poise. Processing parameters are the cooling rate, the heterogeneous nucleation rate and the super cooling temperature interval. The temperature of the glass transition is slightly depend on the cooling rate at each cooling rate the glass will freeze in a different state of internal energy , shown in Fig 2.2. At the melting point T_m the enthalpy H of a crystal includes latent heat of fusion due to long range order. In the case of rapid cooling of the melt, the free energy decreases since long range order do not take place, thus leaving the system at a higher energy rate. Heat treatment, relaxation and stability are thus important considerations in metallic glass. The glass-forming tendency also arises from as size difference between the components in the glassy alloy is a necessary condition for ready glass formation.

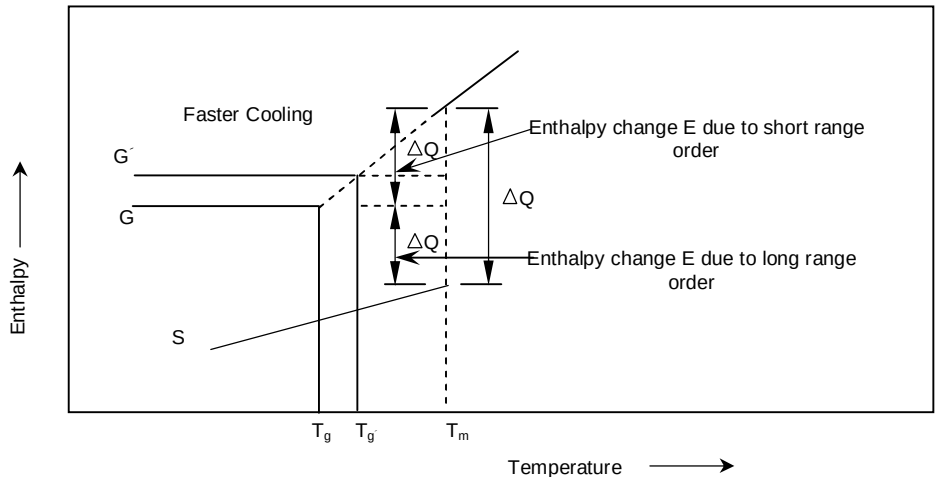

Figure 2.2: Temperature dependence of enthalpy H and G correspond to glass transition and S correspond to the crystalline state

A single parameter that expresses glass forming tendency is the ratio of the glass transition temperature to the melting temperature defined as higher values of τ obviously favor glass formation. For metallic glass to be formed by rapid cooling, $\tau = \frac{T_g}{T_m}$ should be greater than 0.45 by H. S. Chen [9]. Based on alloy composition there are two major groups that rapidly form glasses. In one of these groups the metal is form Fe, Co, Pd, or Pt and the metalloid is B, C, Si, Ge, or P, these metallic glasses constitute soft amorphous magnetic materials.

References

1. Klement, J.W., Willens**,** R.H. and Duwez, P., "Non-crystalline structure in solidified gold-silicon alloys", Nature 187 p869 – 870 (1960)
2. Pond, R. Jr. and Maddin, R, "The solubility of Carbon in Cobalt and Nickel", Trans. Met. SOC. ALME 245 p2475 (1969)
3. Tsuei C.C. and Duwez P. "Electrical Conductivity of Thin Metallic Films with Unlike" Surfaces", J. Appl. Phys. 37, 435 (1966)
4. Alben R, Budnick J.I., Cargil III G.S., Magnetic Glasses (American SOC. for Metals. 304 (1978)
5. Cargil, III, G.S., Solid State Physics, Vol. 30 Ed. Ehrenreich, Academic Press, New York 257 (1975)
6. Masumoto, T., Ohnuma, S., Shirakawa, K., Nose, M. and Kobayshi, K., "Int. Conf. on Liquid and Amorphous Metals", Grenoble, France, 1980
7. Turnbull, D., "Bulk metallic glass matrix composites", Contemp. Phys. 10 p473 (1969)
8. Duwez, P., Willens, R.H. and Klement, Jr. W**.** "Amorphous Metallic Alloys", J. Appl. Phys. 31 p1136 (1960)
9. Chen, H.S., "glassy metals", Rep. Prog. Phys. 23, 43 (1980)

Chapter-3

Theoretical Perspective

In this chapter we have described basic theories which are needed for calculations and the explanation of experimental results. We describe here the theories for Structural, resistivity, magnetization, frequency dependent AC permeability and thermal treatment of $(Fe_{1-x}Mn_x)_{75}P_{15}C_{10}$.

3.1 X-ray Diffraction

Bragg reflection is a coherent elastic scattering in which the energy of the X-ray is not changed on reflection. If a beam of monochromatic radiation of wavelength λ is incident on a periodic crystal plane at an angle θ and is diffracted at the same angle as shown in Fig. 3.1, the Bragg diffraction condition for X-rays is given by

$$2d\,Sin\theta = n\lambda \qquad (3.1)$$

here d is the distance between crystal planes and n is the positive integer which represents the order of reflection. Equation (3.1) is known as Bragg law. This Bragg law suggests that the diffraction is only possible when $\lambda \leq 2d$ [1]. For this reason we cannot use the visible light to determine the crystal structure of a material. The X-ray diffraction (XRD) provides substantial information on the crystal structure.

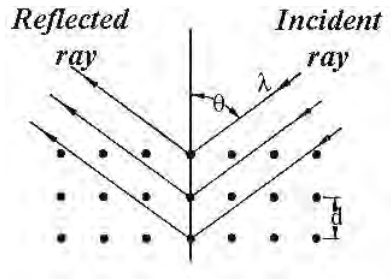

Figure 3.1: Bragg law of x-ray diffraction

3.2 DC Electrical Resistivity

The law of electrical conduction in metals is obtained from Ohm's law which is given by

$$I = \frac{V}{R} \tag{3.2}$$

Where, I is the current, V is the potential difference, and R is the resistance. From laws of resistance, we have

$$R = \rho\frac{L}{A} \tag{3.3}$$

Where, ρ is the resistivity that is the characteristic property of a metal, L is the length and A is the cross-sectional area of the material. Again by the definition of electric field, we know that the electric field, E is

$$E = \frac{V}{L} \tag{3.4}$$

Now putting the values from equations (3.3) and (3.4) into equation- (3.2), we get

$$I = \frac{EA}{\rho} \tag{3.5}$$

In general the current density is defined, as the current per unit cross-sectional area of the specimen, hence, the current density using equation-(3.5), will be as:

$$J = \frac{I}{A} = \frac{E}{\rho} = \sigma E \tag{3.6}$$

Equation (3.6) is another form of Ohm's law, where σ is the electrical conductivity, which is again the inverse of resistivity ρ. Since the dimension of resistivity is ohm-m, so the conductivity σ has dimension $(\text{ohm-m})^{-1}$.

Now we want to express σ in terms of the microscopic properties pertaining to the conduction electrons. These conduction electrons are responsible for the current flow under the influence of electric field because the ions are attached to and vibrate about their lattice sites. They have no net translation motion and hence do not contribute to the current. For the purpose, let us now treat the motion of the conduction electron in

an electric field. In this regard we consider one typical electron. The field exerts a force –eE on the electron. There is also a frictional force due to collision of the form – $m^* \frac{v}{\tau}$, v is the velocity of the electron and τ is a constant called the collision time.

Using Newton's law of motion, we have

$$m^* \frac{dv}{dt} = -eE - m^* \frac{v}{\tau} \qquad (3.7)$$

Where m* is the effective mass of electron. We see that the effect of the collision as usual in friction or viscous forces tends to reduce the velocity to zero. If we consider the steady-state condition for our purpose, then after putting $\frac{dv}{dt} = 0$, the appropriate solution of equation- (3.7) will be as:

$$v = -\frac{e\tau}{m^*} E \qquad (3.8)$$

This is the steady-state velocity of the electron, which is also known as terminal velocity that arises from the friction. It is opposite to the electric field, E because the charge of electron is negative. When a field is applied to a metallic wire/or material under test, there will be two different velocities associated with the electron. The velocity appearing in equation (3.8) is called the drift velocity. This is superimposed on a much higher velocity or speed, known as the random velocity that arises from the random motion of electron like gas even in the absence of electric field. This is due to the fact that the electrons move about and occasionally scatter and change direction. This random motion contributes zero current and also exists in the presence of electric field, but in that case, there is an additional net velocity opposite to the field, as given by equation (3.8) v_d and v, denote these two velocities for distinction. Now the current density can be calculated from equation (3.8). Since there is a charge (–Ne) per unit volume, and since each electron has a drift velocity given by equation-(3.8), it follows that the amount of charge crossing per unit area per unit time is

$$J = -(Ne)v_d = -(Ne)\left(-\frac{e\tau}{m^*} E\right) = \frac{Ne^2\tau}{m^*} E \qquad (3.9)$$

This current is parallel to the electric field, E. Now comparing equation (3.6) and equation (3.9), we get the expression for the conductivity as:

$$\sigma = \frac{Ne^2\tau}{m^*} \qquad (3.10)$$

From equation (3.10), it is seen that σ increases as N increases. This is reasonable because N, the concentration increases; there are more current carriers. The conductivity σ is inversely proportional to m* which is also expected, since the larger m* is, the more sluggish the particle, and harder it is for move. The proportionality to τ follows because τ is actually the time between two consecutive collisions, i.e. the mean free lifetime. Therefore the larger τ is, the more time the electron has to be accelerated by the field between collisions, and hence the large the drift velocity [equation (3.8)], and also the larger σ is. The time τ is also called the relaxation time. To see the reason for this naming, let us apply an electric field to the material long enough for a drift velocity $v_d(0)$ to be established. Now let the field is suddenly removed at some instant. The drift velocity after this instant is governed by the following relation with E=0 as:

$$m^* \frac{dv}{dt} = -eE - m^* \frac{v}{\tau}$$

$$\text{or, } m^* \frac{dv}{dt} = -m^* \frac{v}{\tau} \qquad (3.11)$$

The solution appropriate to the initial condition is now

$$v_d(t) = v_d(0)e^{-\frac{t}{\tau}} \qquad (3.12)$$

Since t is the time between two successive collisions, it may be expressed as:

$$\tau = \frac{l}{v_r} \qquad (3.13)$$

Where l is the distance between two successive collisions and v_r is the random velocity. In terms of these σ becomes:

$$\sigma = \frac{Ne^2 l}{m^* v_r} \qquad (3.14)$$

Let us now discuss the origin of collision time. It seems natural to assume that the frictional force is caused by the collision of electrons with ions. According to this particular model of collision, an electron, as it moves in the lattice, collides with ions,

which has the effect of slowing down the electrons momentum. This model turns out to be untenable because it leads to many points of disagreement with experiment. To cite only one: the mean free path l can be calculated from equation (3.13). If we substitute the values $\tau \cong 10^{-14}$s and $v_r = 10^6$ ms^{-1}, we find that $l = 10^2$Å. This means that, between two collisions, the electron travels a distance of more than 20 times the inter-atomic distance, which one would expect. But in closed-packed structures, in which atoms are densely packed, it is difficult to see how the electrons could travel so far between collisions. This paradox can only be explained by the use of quantum concept. According to quantum mechanics, an electron has a wave character. The De-Broglie relation gives this wavelength in the lattice:

$$\lambda = \frac{h}{m^* v_r} \qquad (3.15)$$

It is well known from the theory of wave propagation in discrete structures that, when a wave passes through a periodic lattice, it continues propagating indefinitely without scattering. The effect of atoms in the lattice is to absorb energy from the wave radiate it back, so that the net result is that the wave continues without modification in either direction or intensity. The velocity of propagation, however, is modified. This is what happens in the case of an electron wave in a regular lattice, except that in this case we are dealing with a matter wave.

3.2.1 Electrical Resistivity

In general, the resistivity is defined as the reciprocal of the conductivity, i.e.

$$\rho = \frac{1}{\sigma} = \sigma^{-1} \qquad (3.16)$$

Using equation (3.10), we get the expression for the resistivity as:

$$\rho = \frac{m^*}{Ne^2} \times \frac{1}{\tau} \qquad (3.17)$$

We know from the interpretation that $\frac{1}{\tau}$ is actually equal to the probability of the electron suffering a scattering per unit time. Thus, if relaxation time is $\tau = 10^{-14}$s, then the electron undergoes 10^{14} collisions in one second. But we see that the electron

undergoes a collision only because the lattice is not perfectly regular. We group the derivations from a perfect lattice into two classes

a. Lattice vibrations (phonons) of the ions around their equilibrium position due to thermal excitation of the ions.
b. All static imperfections, such as foreign impurities or crystal defects.

Among these the latter group we shall take impurities as an example. Now the probabilities of electrons being scattered by phonons and by impurities are additive, since these two mechanisms are assumed to act independently. Therefore, we may write

$$\frac{1}{\tau} = \frac{1}{\tau_{ph}} + \frac{1}{\tau_i} \qquad (3.18)$$

Where the first term on the right is due to phonons and the second term is due to impurities. The former is expected to depend on T and the later on impurities, but not on T. If we now substitute equation (3.18) into equation (3.17), we readily find

$$\rho = \rho_i + \rho_{ph} = \frac{m^*}{Ne^2}\left(\frac{1}{\tau_{ph}} + \frac{1}{\tau_i}\right) \qquad (3.19)$$

From equation (3.19) it is seen that it has split into two terms: a term ρ_i is due to scattering by impurities, which is independent of temperature, called residual resistivity. Another term added to this is ρ_{ph} arises from the scattering by phonons and therefore temperature dependent. This is called ideal resistivity. Furthermore, since crystalline defects serve as scattering centers for conduction electrons in metals, increasing their numbers raises the resistivity. The concentration of these imperfections depends on temperature, composition, and the degree of cold work of a metal specimen. In fact, it has been observed experimentally that the total resistivity of a metal is the sum of the contributions of thermal vibrations, impurities and plastic deformation; that is, the scattering mechanism acts independently of one another. This may be represented in mathematical form as follows:

$\rho = \rho_i + \rho_{ph} + \rho_d$ (Plastic deformation causes by the magnetic annealing) (3.20)

At low temperature, scattering by phonons is negligible because the amplitudes of oscillations are very small; in that region $\tau_{ph} \rightarrow \infty$, $\rho_{ph} \rightarrow \infty$ and hence $\rho = \rho_i$ is a constant. As temperature increases, scattering by phonons becomes more effective and $\rho_{ph}(T)$ increases; this is why ρ increases. When temperature becomes sufficiently large, scattering by phonons dominates and $\rho \cong \rho_{ph}(T)$. In the high-temperature region, $\rho_{ph}(T)$ increases linearly with temperature. The part of ρ which is independent of temperature is called Matthiessen rule. From equation (3.20), it is expected that ρ_i is proportional to the impurity concentration N_i. Resistivity linearly increases with temperature up to the melting point for the case of pure element.

3.3 Magnetoresistance

The magnetoresistance refers to the change in electrical resistance of a specimen in response to the magnetic field applied to the specimen externally. The resistance change occurs with the magnetic field when the field is sufficient enough to change the orientation of the electrons of the atoms. In that case the path of the electron becomes curved and do not go exactly in the direction of the superimposed electric field. The change of orientation of the atomic electrons occurs such that the conduction electron find more mean free path with less number of collision with the atomic ions and the atomic electrons, then the resistance decreases other wise it increases or remain constant. When the resistance of a material changes with the application of the magnetic field then the material is said to have the magnetoresistance. The magnetoresistance usually expressed in percentage and is calculated by the following way

$$MR\% = \frac{R(H) - R(0)}{R(0)} \times 100\% \qquad (3.21)$$

Where, R (H) is the resistance in presence of magnetic field and R (0) is the resistance in absence of magnetic field.

All metals show some MR, but up to only a few percent. Nonmagnetic metals such as Au, exhibits small MR, but the magnitude is somewhat greater (up to 15%) in ferromagnetic metals such as Fe and Co. The semimetal Bi also shows ~18% MR in a transverse field of 0.6T which rises to a 40fold change at 24T [2]. Cu is more typical

in the same very powerful field (24T) gives rise to change of only ~2% at room temperature. This is the classical positive magnetoresistance that varies as B^2 (B=applied magnetic field) in half metallic ferromagnets such as CrO_2, Fe_3O_4 at low temperature [3]. It is absent in the free electron gas [4] but appears when the fermi surface is non spherical. This MR originates from the impact of the Lorentz force on the moving charge carriers similar to the Hall Effect. Its value is ~10% at 10T. A classification of magnetoresistance phenomenon is based on the distinction familiar in magnetism between intrinsic composition and purity and extrinsic properties of the sample.

The phenomenology of the magnetoresistance effect is similar to that of magnetostriction. This effect can be classified into two categories: one is the part, which depends on the intensity of spontaneous magnetization that corresponds to the volume magnetostriction. The second is that change caused by the rotation of spontaneous magnetization, which corresponds to the usual magnetostriction. Mott interpreted this phenomenon in terms of the scattering probability of the conduction electrons into 3d holes. If the substance is in a ferromagnetic state, half of the 3d shell is filled up, so that the scattering of 4s electrons into the plus state of 3d shell is forbidden. This scattering is however, permitted in a nonmagnetic state in which both the plus spin state and the minus spin state of the upper 3d levels are vacant. Mott explained the temperature variation of resistivity fairly well by this model Kasuya interpreted this phenomenon from a standpoint quite different from Mott theory. He considered that d electrons are localized at the lattice points and interact with the conduction electrons through the exchange interaction. At 0^0K the potential for the conduction electron is periodic, because the spin of 3d electrons of all the lattice points in the same direction. At finite temperature, spins of 3d electrons are thermally agitated and the thermal motion may break the periodicity of the potential. The 4s electrons are scattered by an irregularity of the periodic potential which results in additional resistivity. Kasuya postulated that the temperature dependence of the resistivity of ferromagnetic metal is composed of a monotonically increasing part due to lattice vibration and an anomalous part due to magnetic scattering, the magnitude of the later being explained by this theory. The effect of high temperature has been treated in two different approaches. The first approach is given by Harris *et. al*. [5]

considers a constant exchange interaction between magnetic atoms and a random distribution of the local anisotropy field is considered which changes with temperature. The other approach is to consider a distribution of exchange integral is assumed in order to take into account the fluctuation in the amorphous alloys as taken by Handrich [6]. Both the approaches are unrealistic and in fact no rigorous theory of the high temperature behavior for amorphous material has been developed.

3.4 Hall effect

The ordinary Hall effect was discovered in 1879 by Edwin Hall. It refers to the difference in potential produced on the opposite sides of a conductor when a current is flowing in the presence of a magnetic filed applied perpendicular to the current. The effect arises from the Lorentz force acting on a moving charge in a magnetic field that curves its trajectory away from its straight-line path. This causes charge to accumulate on one side of a conductor and create a potential difference across the opposite sides of a conductor. If one connects the sides to another conductor, a current transverse to the initial current flows though it, which is called a Hall current. In this way the Hall effect is viewed as a source for transverse electromotive force (EMF), a kind of generator. Other origins for the Hall effect which included the asymmetric scattering (known as skew scattering) from impurities with spin-orbit coupling and a more esoteric quantum mechanical effect arising from the time delay in scattering events that in the presence of spin-orbit scattering produced a “side jump”, i.e., when one traced the path of a scattered electron back to the scattering region it was displaced to one side of the scattering center [7]. There are indeed two different manifestations of spin-orbit scattering contributing to the additional Hall effects (called the extraordinary Hall effect). The first is skew scattering and the second is the side jump which arises not only from spin-orbit scattering of impurities, but also from ordinary scattering when the electron conduction wave functions have their spin and orbit coupled together.

3.5 Differential Thermal Analysis (DTA)

DTA means the differential thermal analysis. Differential thermal analysis is the process of accurately measuring the difference of temperature in between the test sample and the reference when both are being heated or cooled at the same rate under, identical environment. Differences in temperature between the test sample and reference may arise, when physical or chemical changes take place in the test material. The change of temperatures are observed either by endothermic or exothermic peak as a function of time or temperature. These changes may due to dehydration, transition from one crystalline variety to another, destruction of crystalline lattice, oxidation, hydrogenation, melting and boiling of the materials etc. Hence reference is used as a baseline which is thermally stable and uncreative i.e. no reaction can take place with in the ref. sample.

3.5.1 The endothermic reaction

Reactions are accompanied by the absorption of heat is known as endothermic process or reactions. Reactions of this type require a continuous supply of energy from the outside to keep them going. For example, the decomposition of potassium chlorate into potassium chloride and oxygen will take place only so long as the compound is heated from outside. Similarly, the reaction of hydrogen and iodine to from hydro-iodic acid takes place with absorption of heat.

e.g.	$H_2 + I_2$	=	2HI	1.2 kcal.
	C + 2S	=	CS_2	1.5 kcal.

The compounds which are formed by endothermic reactions, such hydrogen peroxide, H_2O_2 and hydro-iodic acid, HI, are thermally unstable. This means that the internal energies of the molecules of H_2O_2 and HI tend to break the bonds holding the atoms together.

3.5.2 The exothermic reaction

The reactions which are accompanied by the evolution of heat, is known as the exothermic reaction. Exothermic reaction may proceed in the absence of any supply

of energy from outside. The burning of magnesium, carbon, methane, etc, in air, are all exothermic reactions.

e.g. $C + O_2 = CO_2 + 97$ kcal.

$2Mg + O_2 = 2MgO + 148$ kcal.

Thus, carbon will continue to burn in oxygen with the evolution of heat until the supply of carbon or oxygen is exhausted. It may be noted here that compounds which are formed by highly exothermic reactions, such as carbon dioxide, magnesium oxide, are stable towards heat. These are said to be thermally stable. This means that a very high temperature is required to separate them into their component elements.

3.5.3 Peak Area, Peak Temperature

When no reaction occurs in the specimen then no temperature difference between the specimen and the reference sample is observed but as soon as a reaction commences the specimen becomes hotter or cooler than the inert material and a peak develops on the curve for temperature difference against time ($\Delta T/t$) or temperature ($\Delta T/T$). Along the line AB the difference is zero since no reaction is occurring but at B an endothermic reaction starts and gives rise to the peak BCD with its minimum at C, where, the rate of heat absorption by the reaction is equal to the difference between the rate of supply of heat to the specimen and to the inert material. Peak area (BC $\times$ DE) is proportional to the amount of reacting material. The distance BD is usually referred as the peak width and the distance EC as the peak height or amplitude

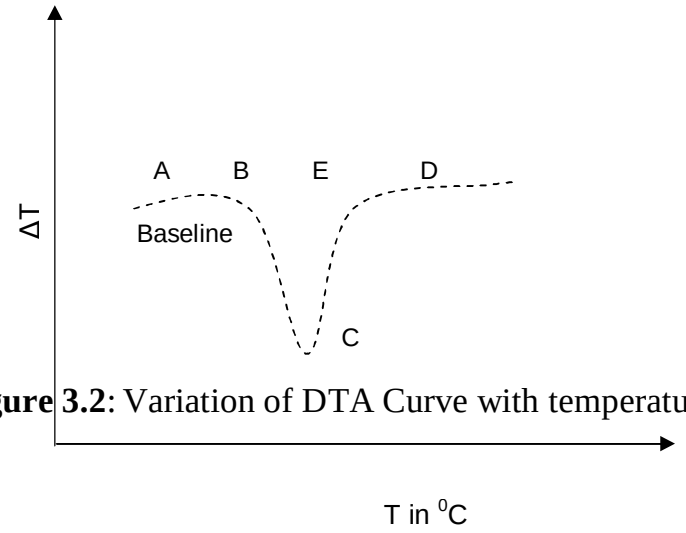

Figure 3.2: Variation of DTA Curve with temperature

The area enclosed by the peak has to be accurately determined for quantitative work. In this method two tangents are drawn on both sides of the peak and a straight line AB joined the points of tangency. The area enclosed by ABC formed the peak area.

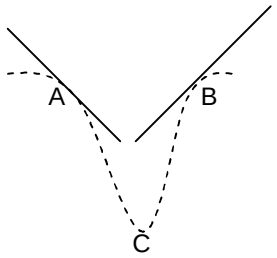

Figure 3.3: DTA endothermic peak analysis of the sample

3.5.4 Effect of heating rate

Peak area increases with rapid change of temperature (i.e. rate of heating). Peak shape change with finer particle size to more reaction centers. The random stacking of the layers, coupled with disruption caused by removal of inter layer water, would be expected to expose more nuclei to dehydration at any moment for a given weight of mineral as slow heating rate reduces the sharpness of the peaks unduly and very fast rates tend to cause overlapping of neighboring reactions.

3. 5.5 Transition state

A chemical reaction is presumably a continuous process involving a gradual transition from reactants to produce an arrangement of atoms at an intermediate stage of reaction as though it is an actual molecule. This intermediate structure is called the transition state. The reaction sequences are as follow.

Reactants ⟶ Transition state ⟶ Products

ΔH is the difference in energy content between reactants and products, so E_{act} is the difference in energy content between reactant and transition state.

3.5.6 Activation Energy, E_{act}

The minimum amount of energy that must be provided by a collision for reaction to occur is called the activation energy. It is denoted by E_{act}. When heat is liberated, the heat content enthalpy H of the molecules them selves must decrease, the change in heat content. ΔH is therefore given a negative sign. (In the case of an endothermic reaction, where heat is absorbed, the increase in heat content of the molecules is indicated by a positive ΔH)

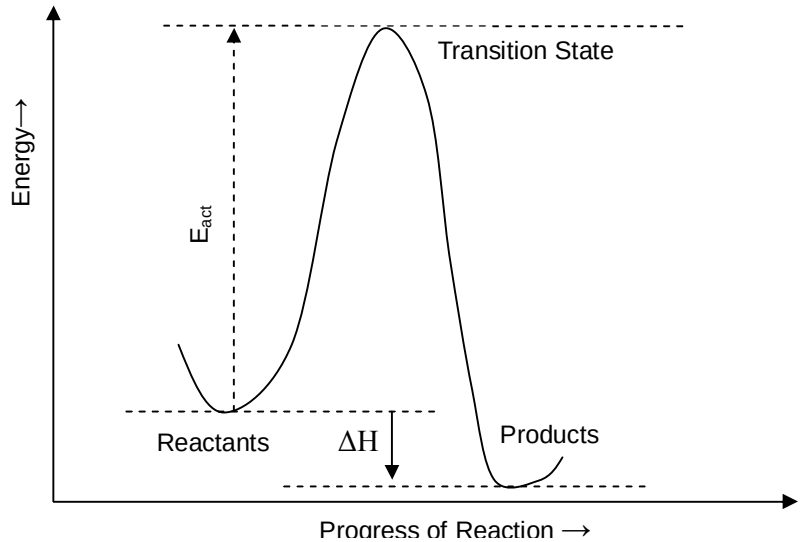

Figure 3.4: Activation energy for a reaction to start in DTA experiment

3. 5.7 Change of Phase

A change of phase or phase change occurs when a crystalline solid becomes liquid or when a liquid becomes a vapor, or when the reverse of either of these processes takes place.

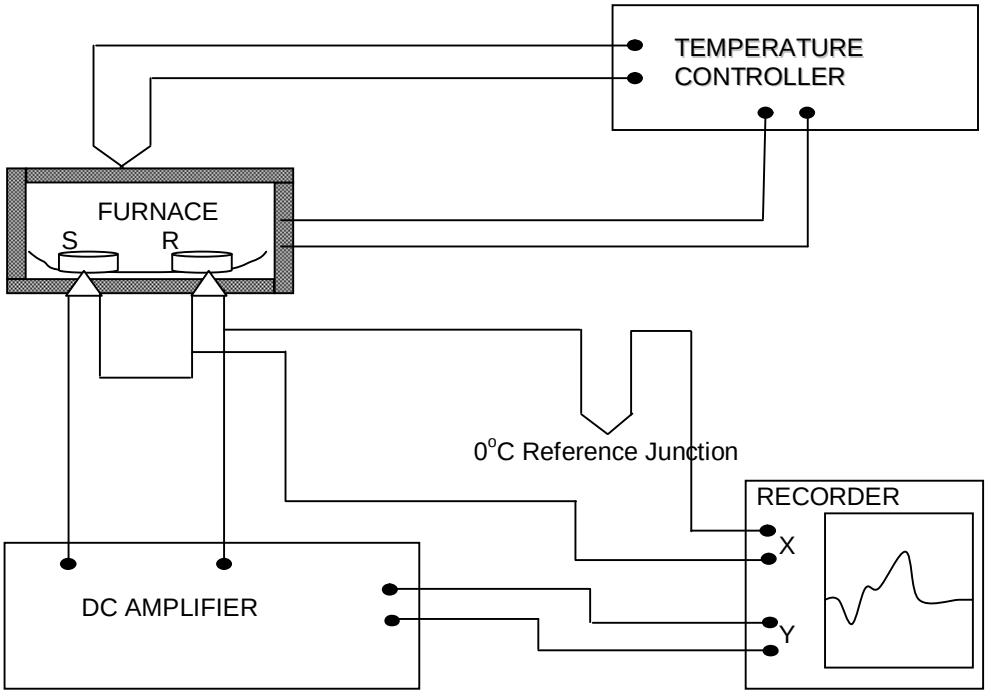

Figure 3.5: A Schematic diagram of the DTA assembly.

3.5.8 Experimental set-up of the DTA apparatus

- DTA assembly consists of a sample holder to place the sample.
- Thermocouples for measuring temperatures.
- A furnace to heat the sample
- A program controller to heat the sample at a uniform rate.
- And a recorder for registering the temperature difference between the sample and the reference material.

3.6 Thermo Gravimetric Analysis (TGA)

The thermo Gravimetric analysis (TGA) are often called TG% and been done with the experiment of DTA at the same time to compare the result of DTA and TG% to find out more accurately what happened in the test material at each rising temperatures. The TG% means the mass loss or mass gain at different temperatures often calculated at percentages. The TG% results are usually shown in graphical mood in which the temperature or time is plotted against mass change in percentage. When any reaction occurs, the reaction may be endothermic or exothermic may also associated with mass change due to evaporation of fundamental element from the sample or may be the mass gain due to new formation of compound. The TG% peak helps to analyze the DTA curves more accurately.

3.7 Differential Thermo Gravimetric (DTG)

DTG calculates the rate of mass change at any temperature with respect to the differential change of temperature or time at that temperature. This calculation is done in association with a TG% analysis. It is done for the following reason. Some time in TG% curve, there may be one peak due to two or more successive reactions that happens with in a very short time interval and that cannot be detected with the TG peak. TG% gives one peak for very close successive reactions. On the other hand the DTG peaks are so useful tool that it can differentiate very clearly that closed reactions with giving separate peaks for each of the successive reactions. In DTG analysis the $\frac{dm}{dT}$ is plotted against Temperature T or time t in the other axis. At the peak the rate of mass loss/gain is maximum. The area under the DTG peak is proportional to the mass change *dm*. Height of the peak at any time or temperature indicates the rate of mass change at that temperature

3.8 Experimental set up for magnetization measurement

3.8.1 The principle of VSM

The vibrating sample magnetometer has become a widely used instrument for determining magnetic properties of a large variety of materials: diamagnetic, paramagnetic, ferromagnetic and antiferromagnetic. The method was developed by

Foner [8] and on the flux change in a coil when the sample is vibrated near it. It has a flexible design and combines high sensitivity with easy of sample mounting and exchange. Samples may be interchange rapidly even at any operating temperature. Measurements of magnetic moment are small as 5×10^{-5} emu /g are possible in magnetic fields from zero to 4 Tesla. Maximum applied fields of 2- Tesla are reached using conventional laboratory electromagnets. Vibrating sample magnetometers normally operate over a temperature range of 20 to 1050 K

When the sample of a magnetic material is placed in a uniform magnetic field, a dipole moment proportional to the product of the sample susceptibility times the applied field is induced in the sample. If the sample is made to undergo a sinusoidal motion, and electrical signal is induced in suitability located stationary pick- up coils. This signal which is at the vibrating frequency, is proportional to the magnetic moment, vibration amplitude and vibration frequency. In order to obtain the reading of the moment only, a capacitor is made to generate another signal for comparison which varies in its moment, vibration amplitudes and vibration frequency in the same manner as does the signal from the pick up coil. These two signals are applied to the inputs of a differential amplifier, and because the differential amplifier passes only difference between the two signals, the effect of vibration amplitude and frequency changes is cancelled. Thus only the moment determines the amplitude of the signal at the output of the differential amplifier. This signal is in turn applied to a lock –in amplifier, where it is compared with the reference signal which is at its internal oscillator frequency and is also applied to the transducer which oscillates the sample rod. Thus the output of the lock in amplifier is proportional to the magnetic moment of the samples\ only avoiding any noise of frequency other that of the magnetic moment of the signal. The absolute accuracy of this system is yields an accuracy of 0.05% of full scale. The absolute accuracy of this system is better than 2% and reproducibility is better than 1%. Least measurable moment is $5X10^{-4}$emu. Variation magnetic field is achieved with a Newport Electromagnet Type 177 with 17.7 cm diameter pole pieces. The magnet is mounted on a graduated rotating base. The standard model is modified to provide an adjustable pole gap in order that the highest possible field strength is available. The field can vary from 0 to 1T. The field is measured directly by using Gauss meter.

3.8.2 Electronic circuits of the VSM

The function of the associated electronic circuits is

(i) To permit accurate calibration of the signal out put from the detection coils.

(ii) To produce a convenient AC output signal which is directly related to the input and which can be recorded

(iii) To produce sufficient amplification for high sensitivity operation.

The block diagram of the electronic circuit used for the vibrating sample magnetometer (VSM) consists of a mechanical vibrator, a sine wave generator, an audio amplifier, a ratio transformer, a phase- shifter, a lock in amplifier, 4 pick up coils system, a reference coil system, an electric power supply, an electromagnets and PID regulator as shown in figure:

The sample magnetized by the electromagnet generates an e.m.f. in the pick up coils PC. The strength of this signal is proportional to the magnetization of the sample. The vibrating permanent magnet also generates an e.m.f. of fixed amplitude in the surrounding reference coils. This reference signal is stepped down with the help of a ratio transformer so that its amplitude is equal to that sample signal. The two signals are then brought in phase and put to the lock in amplifier. The lock in amplifier works as a null detector. The ratio transformer reading is to be calibrating using spherical shape sample S of 99.99% pure nickel. The circuit diagram of VSM as shown bellow fig 3.6.

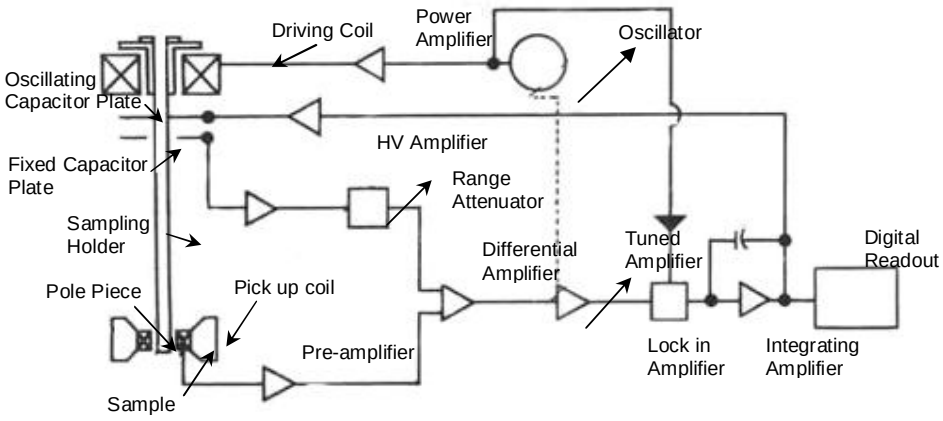

Figure. 3.6 Block diagram of Vibrating Sample Magnetometer

3.8.3 Sensitivity limits

Limits of sensitivity are determined by signal to noise ratio at the input circuit, where noise is defined as any signal not arising from the magnetic moment of the sample. The major sources of noise are the Johnson noise of the wire used for the pick up coils and the magnetic responses of the sample holder, which superimposes undesired signals in phase with the wanted signal. Use of a minimum mass of weakly diamagnetic materials for a sample holder, carefully checked to contain no ferromagnetic impurities, is essentials to minimize this coherent noise contribution. Corrections for the small magnetic contribution of the samples holder can then be made by measurements with the sample removed. This correction is much less than the equivalent case with a moving coil system.

We used a standard sample for the calibration was spherical shaped specimens of mass 152mg of pure nickel (99.99%).

3.8.4 Stability tests differential measurements

With only the lock – in amplifier and the oscilloscope as a null detector, it was found that that 152mg Ni sample signal could be balanced reproducibility. Such reproducibility indicated that the long time drifts caused by the combined effects of vibration, amplitude changes and frequency changes a bridge sample position and offer effects were negligible. Chosen synchronous phase detector added differential changes about one- tenth the size that could be recorded reproducibly.

3.8.5 Vibration amplitude

The pick- to –pick vibration amplitude has been varied from less than o.1mm upto 1.0 mm in order to examine errors caused by amplitude changes, such tests show that the measured magnetic moment varied by less than 0.5% over these range of amplitude, although at higher variation of amplitudes , because of the larger signals involved.

3.8.6 Vibration frequency

The vibration frequency is not critical. High frequency operational is limited by the driving mechanism and capacitive shunting in the detection coils. Frequencies of 100Hz or less permit the use of inexpensive components and minimize eddy current shielding by the vacuum chamber. The measurements are completely independent of eddy currents in the surrounding parts, if the measurements and calibration are made at the same temperature. The thickness of conducting parts has been minimized, so that the temperature dependence of penetration depth is less than 1%.

3.8.7 Vibration Problems

Mechanical coupling between the vibrating system and the fixed detection coils must be avoided. Although the coils are arranged for minimum sensitivity to external vibration, a noticeable background signal is obtained when the vacuum chamber contacts the detection coils. Such mechanical effects are difficult to eliminate electronically, because the spurious background signal has the same frequency as the sample signal and maintains a constants phase differences with respect to the sample signal. Usually the magnetometer and detection coils are both supported by the magnetic coupling, so that some mechanical coupling may be noticed as highest sensitivity.

3.9 Complex Permeability Measurements

Permeability is the degree of magnetization of a material that responds linearly to an applied magnetic field. Magnetic permeability is represented by the symbol μ. This term was coined in September, 1885 by Oliver Heaviside.

In SI units, permeability is measured in henrys per metre, or newtons per ampere squared. The constant value μ_0 is known as the magnetic constant or the permeability of vacuum. The permeablity can be given as

$$\mu = \frac{\vec{B}}{H} \qquad (3.26)$$

Where, B is the magnetic flux density produced by the magnetizing force H.

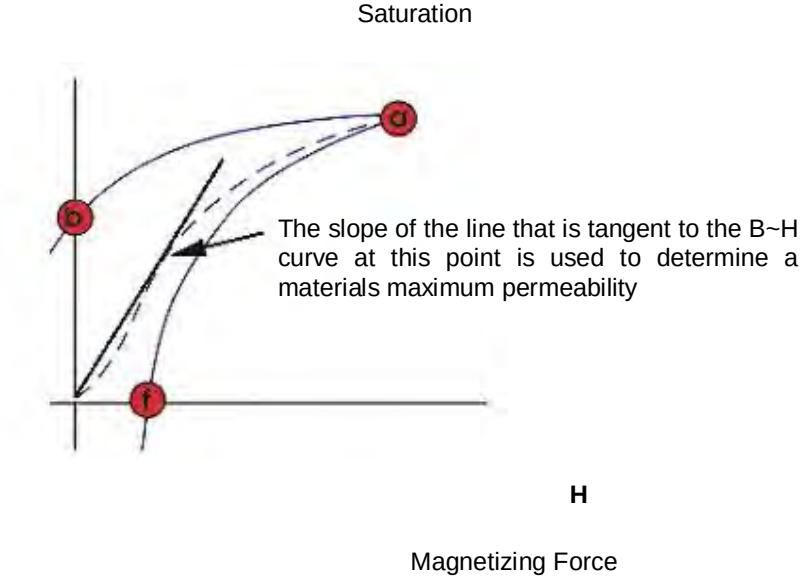

Figure-3.7: B~H Curve illustrates the procedure to determine the permeability

It is clear that this equation above describes the slope of the curve at any point on the hysteresis loop. The maximum permeability is the point where the slope of the B~H curve for un-magnetized material is the greatest. This point is often taken as the point where a straight line from the origin is tangent to the B/H curve. The relative permeability is defined as the ratio of the material's permeability to the permeability in free space.

$$\mu_r = \frac{\mu}{\mu_0} \qquad (3.27)$$

Where, $\mu_0 = 4\pi \times 10^{-7} H/m$

The measurement of permeability has significant role to detect hard magnetic materials as well as soft magnetic materials. For hard magnetic materials, the value of the relative permeability is low that in turn leads to have high coercive field. On the other hand, the high permeability is the indication of soft magnetic materials that in turn leads to have low coercive field.

The above discussion on permeability is only considering the application of static fields. The dynamic response of the magnetic domains to the external field determines the complex permeability. The value of complex permeability provides the information about the inertia of the domains, their distribution and mutual coupling. The phase lag between the applied field and the response of magnetic domains determine the real μ' and imaginary μ'' parts of the complex permeability.

As the desirable properties for soft magnetic materials are high permeability and low loss so we have to consider the losses and resonance, which affect the permeability of soft magnetic materials in various ranges of frequencies. If a magnetic material is magnetized by the alternating magnetic field, $H = H_0 e^{j\omega t}$, that magnetic flux density of B is generally delayed by the phase angle δ because of the presence of loss and is thus expressed as $B = B_0 e^{j(\omega t - \delta)}$. The permeability is then will be a complex one and can be expressed as:

$$\mu = \frac{B}{H} = \frac{B_0 e^{j(\omega t-\delta)}}{H_0 e^{j\omega t}} = \frac{B_0}{H_0} e^{-j\delta} = \mu' - j\mu'' \qquad (3.28)$$

where, μ′ is the real part which is actually the energy storage part and μ″ is the imaginary part which is called loss factor. This complex permeability is then related to two different magnetizing mechanisms. One is the spin rotational magnetization and the other is the domain wall motion. In order to explain, we can consider the hysteresis loop, which is the magnetization trace owing to the alternating magnetic field, applied to the sample. This hysteresis implies the existence of energy losses in the system and these loses is proportional to the area of the loop.

3.9.1 Techniques for the Permeability Measurement

Measurements of permeability normally involve the measurements of the change in self-inductance of a coil in presence of the magnetic core. The behavior of a self-inductance can now be described as follows. We assume an ideal loss less air coil of inductance L_0. On insertion of a magnetic core with permeability μ, the inductance will be μL_0. The complex impedance Z of this coil can be expressed as follows:

$$Z = R + jX = j\omega L_0 \mu = j\omega L_0 (\mu' - j\mu'') \qquad (3.29)$$

where the resistive part is

$$R = \omega L_0 \mu'' \qquad (3.30)$$

and the reactive part is

$$X = \omega L_0 \mu' \qquad (3.31)$$

The RF permeability can be derived from the complex impedance of a coil, *Z*, given by equation (3.29). The core is taken as toroidal to avoid demagnetizing effects. The quantity L_o is inductance of the winding coil without the sample core.

References

1. Kittel, C., “Introduction to Solid State Physics”, 7th edition, Jhon Wiley & Sons, Inc., Singapore (1996).
2. Pippard, A.B., “Magnetoresistance” Cambridge University Press Cambridge UK (1984)
3. Watts S.M, Wirth S, Von Molnar S, Barry F, and Coey JMD, “Evidence for two-band magnetotransport in half-metallic Cromium oxide”, Phys Rev B61, 149621 (2000).
4. Ashcroft N, and Mermin B, “Solid State Physics” Holt Richart and Winstone New York (1976)
5. Harris, R., Phischke, M. and Zucherman, M., “New Model for Amorphous Magnetism”, J. Phys. Rev. Lett. 31 p160 (1973)
6. Polak, Ch., Knobel, M., Grossinger, R., Sato Turtell, R., “The development of nanocrystalline $Fe_{13.5}$-Nb_3-$Si_{13.5}$-B_9, Magnetism and Structural disorder”, J. Magn. Magn. Mater. 134 p1 (1994)
7. Berger, L. and Bergmann, G., “The Hall Effect and Its Applications”, Eds. C.L. Chien and C.R. Westgate (Plenum, New York, 1979) p55
8. Forner, Simon, “Vrsatile and Sensitive Vibrating Sample Magnetometer”, Rev. Sci. Instr., 30, 548 (1959)

Chapter-4

EXPERIMENTAL TECHNIQUES

The structural property of $(Fe_{1-x}Mn_x)_{75}P_{15}C_{10}$ samples have been investigated through X-ray diffraction (XRD) experiment. The transport properties have been investigated through measurements of normal electrical resistivity, temperature dependence resistivity, Hall resistivity and the magnetoresistance of the material. The magnetic properties carried out by the measurement of magnetization, AC permeability and the thermal property was carried out by DTA, TGA and DTG measurements.

4.1 Resistivity Measurement Technique

There are various types of electrical methods for resistivity/conductivity measurements. The technique, that has been used here to measure the resistance of the Metallic glass ribbon a conventional 4-probe technique

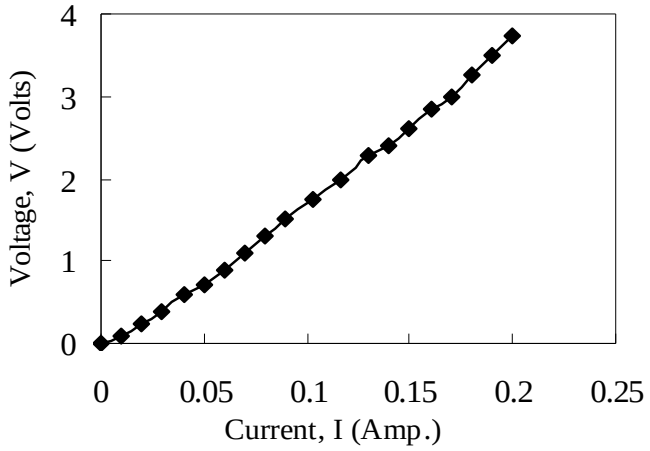

Figure 4.1: I~V Curve for the determination of resistance

The current (0-0.20A) passed through the sample and the corresponding voltage was measured. The resistance is then calculated from the slope after fitting the trend (straight) line to *I~V* curve as shown in figure-4.1

In this method, two of the probes have been used to measure the potential difference between two points, while the other terminals were used to pass current through the sample as shown in figure-4.2. For the electrical contacts silver glue has been used in the present work to avoid the difficulty. In this case the spacing between inner probes has been taken as effective length, l to calculate the resistivity as:

$$\rho = R \times \frac{A}{l} ohm - meter \qquad (4.1)$$

where, R is the resistance of the sample, A is the cross-sectional area, which is the product of the width and thickness.

However, to measure the resistivity as a function of temperature and Hall resistivity, this 4-probe method has been used with the following experimental setup, and those are discussed here separately:

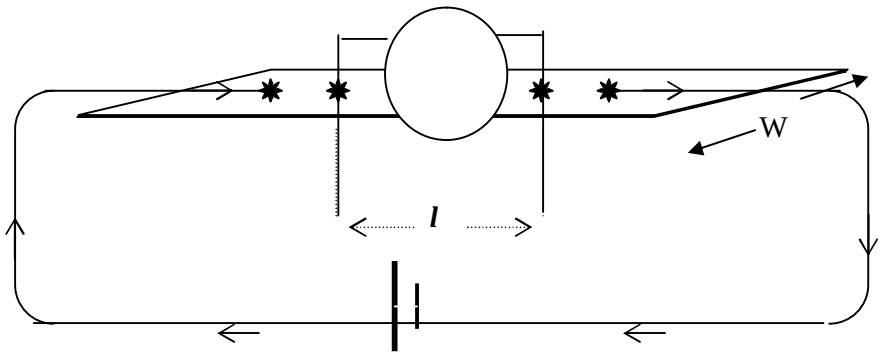

Figure-4.2: 4-probe technique to measure resistivity

4. 1.1 Room Temperature resistivity measurements

Figure-4.2 shows the schematic diagram of experimental setup for resistivity measurement at room temperature (298K). Current (0 mA to 200 mA with an interval of 10 mA) passed through the sample from the regulated power supply in c.c mode; corresponding voltage across the inner two probes has been recorded by the digital voltmeter.

4.1.2 Temperature dependence resistivity measurement

Figure-4.3 shows the experimental setup for low temperature (93K to 298 K) resistivity measurement. We prepared this set up for four probe method to measure low temperature transport property. In this set up both the sample and the thermocouple were attached in the sample holder and downed slowly in the liquid nitrogen container. When the reading of the digital voltmeter reached in milivolt at the desired temperature that was recorded from chromel Constantan temperature calibration chart. At this position (0 mA to 200 mA with an interval of 10 mA) current passed through the sample from the regulated power supply in c.c mode and the corresponding voltage across the inner two probes has been recorded by the digital voltmeter. This procedure is repeated from 93K to 298K with interval 10K. From this recording data we have calculated low temperature resistivity of the samples.

Figure 4.3: Low temperature resistivity measurement setup

4.2 Magnetoresistance Measurement

Magnetoresistance measurement is done by the calculation method from the resistivity, measured by the standard 4-probe method as discussed in section 4.2. By the definition of magnetoresistance, it is given by

$$MR(\%) = \frac{\rho(H) - \rho(H=0)}{\rho(H=0)} \times 100 \qquad (4.2)$$

Where $\rho_{H=0}$ is the resistivity at magnetic field, H=0 kilogauss and $\rho_{H=x}$ is the resistivity at magnetic field, H=x (x=0-0.57) T corresponding to current (0-8) Amp.

4.3 Hall effect measurement

The Hall-coefficient is related to the electric field in the y-direction, E_y the x-directed the electric current density, J_x and the component of the magnetic field in the z-direction, H_z by the relation:

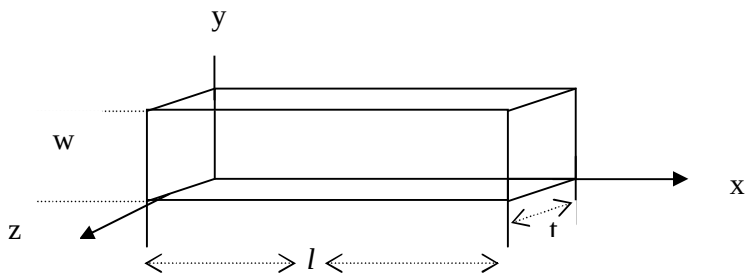

Figure 4.4: Hall resistivity measurement

$$R_H = \frac{E_y}{J_x B_z} \qquad (4.3)$$

Consider a specimen with the geometry as shown in figure-4.7. Three quantities must be measured, Magnetic field, H_z *along* the z direction, Voltage developed, Vy along the y direction and Current, I along the x direction. The current density can be determined by dividing the total current by the cross-sectional area of the sample. Thus $H_z=H$; $J_x=1/wt$ and $E_y=V_y/t$,

$$R_H = \frac{wV_y}{IH} \qquad (4.4)$$

where, *t* is the thickness and w is the width of the sample. In case of thin film, the working formula for calculating the Hall coefficient, R_H reduces to:

$$R_H = \frac{wR}{H} \qquad (4.5)$$

Where R is the resistance measured by the 4-probe method.

The Hall resistivity is $\rho_H = R_H x\ A/L$ (4.6)

4.4 DTA, TGA and DTG measurements

For the investigation of thermal response of the ribbons we have taken DTA, TGA and DTG of the ribbons. For this purpose we have used the lab facility of Bangladesh Council of Scientific and Industrial Research, Dhaka

4.5 Magnetization measurement

Magnetization is the magnetic moment per unit volume. There are various ways of the measuring of magnetization. In the present work, magnetization was measured by using a Vibrating Sample Magnetometer (VSM) at room temperature with covering a wide range of magnetic field. The sample, usually a sphere or small disc, is cemented to the lower end of a rod, the other end of which is fixed to a mechanical vibrator. Current through the vibrator and vibrate the rod at about 37cycle/sec with amplitude of about 7/pp in a direction at right angles to the magnetic field. The oscillating magnetic field of the sample induces an alternation emf in the direction coils. The vibrating rod also carries a reference specimen, in the form of a small permanent magnet near its upper end, the oscillating field of this induces another emf in two reference coils. The two voltage form two sets of coils are compared, and the difference is proportional to the magnetic moment of the sample. The magnetization measurement was performed (0-0.3)T magnetic field for all samples.

Figure 4.5: Vibrating Sample Magnetometer

4.5.1 Calibration of the VSM

There are usually two methods of calibration of a vibrating magnetometer

(i) by using a standard sample and

(ii) by using a coil of small size whose moment can be calculated from the magnitude of the d.c current through it.

We have calibrated the V.S.M. using a 152mg spherical sample of 99.99% pure nickel. The sample was made spherical with the help of the sample shaping device. The saturation magnetic moment of the sample has been calculated using available data. The ratio transformer reading is obtained by actual measurement from the relation

$$M=KK^{/} \qquad (4.7)$$

Where M is magnetic moment, $K^{/}$ is saturation ratio transformer reading and K is VSM calibration constant. But

$$M=m\sigma \qquad (4.8)$$

Where, σ is the specific magnetization and m is the mass of the sample. From (4.7) and (4.8) calibration constant is given by

$$K=m\sigma/K^{/} \qquad (4.9)$$

The accuracy of this calibration, however, depends on the reliability of the standard nickel sample, the accuracy of the ratio transformer and the gain of amplifier. The equipment has been operated repeatedly with the same standard sample and stability has been found to be within 1 part in100.

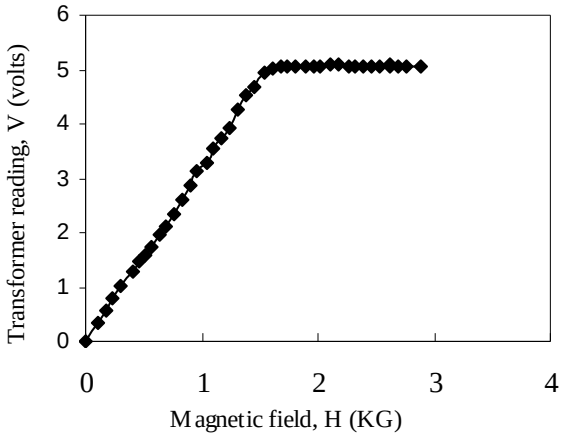

Figure 4.6: Calibration graph for vibrating sample magnetometer

The absolute accuracy of the instrument depends on the knowledge of the magnetic properties of the calibration standard and reproducibility of the sample position. When the substitution of calibration is used, the major error ± 1% is introduced by the estimation of standard nickel sample. The relative accuracy of these instruments depends on accurate calibration of the precision resistor divider net work.

The total error here can be kept less than 0.5%. A typical calibration curve of magnetic field Vs ratio transformer reading is shown in fig.4.6

Calibration Data

(i) Sensitivity =100μV

(ii) Reference phase =89.9°

(iii)Time constant =1s

(iv) Peak to peak voltage =7V

(v) Bandwidth =12dB

(vi)Reference frequency, f =37Hz

(vii) Mass of the pure nickel sample,m =152x10^{-6} kg

(viii)Bohr magnetron, s =58.5 Am^2/kg

(ix)) Ratio transformer reading, $K^{/}$ =5.05V

(x) Saturation magnetic field= 1.8KG and

Putting the of m, $K^{/}$ and s values in eq^n. (5.3) we get

K= 152x10^{-6}x58.5/ 5.05

= 1.760 emu/V

The magnetization of the ribbons samples were calculated by using the following eq^n (4.10)

$$M = \frac{KV}{m} \quad \text{emu/g} \qquad (4.10)$$

Where, M= Magnetization of the experimental sample

m= Mass of the experimental sample

V= Voltage correspond to the magnetization

K= Calibration constant of the VSM.

The relation between the saturation magnetization, M_s at 0°K and the number of Bohr magnetrons, n_B per molecule $(Fe_{1-x}Mn_x)_{75}P_{15}C_{10}$

$$n_B = \frac{M}{5585} \times Ms \qquad (4.11)$$

Where, M is the molecular weight of the substance [3].

4.6. Permeability Measurement

The frequency characteristics of $(Fe_{1-x}Mn_x)_{75}P_{15}C_{10}$ samples i.e. the initial permeability spectra were investigated using an Agilent Impedance Analyzer (model no. 4294A as shown in Fig. 4.6). The complex permeability measurements on toroid shaped specimens were carried out at room temperature on all the samples in the frequency range 1 kHz - 13 MHz. The real part $(\mu_i^{/})$ and imaginary part $(\mu_i^{//})$ of the complex permeability were calculated using the following relations

$$\mu_i^{/} = L_s / L_0 \text{ and} \qquad (4.12)$$

$$\mu_i^{//} = \mu_i^{/} \tan\delta$$

where L_s is the self-inductance of the sample core and $L_0 = \mu_o N^2 S / \pi\bar{d}$ is derived geometrically. Here L_o is the inductance of the winding coil without the sample core, N is the number of turns of the coil (N = 5), S is the area of cross section of the toroidal sample as given below:

$$S = d \times h,$$

where $$d = \frac{d_2 - d_1}{2},$$

d_1 = Inner diameter,

d_2 = Outer diameter,

h = Height

and $\bar{d}$ is the mean diameter of the toroidal sample as given below:

$$\bar{d} = \frac{d_1 + d_2}{2}$$

The relative quality factor is determined from the ratio $\frac{\mu_i^{/}}{\tan\delta}$.

Figure 4.7: Agilent impedance analyzer

Reference

1. Shukla, S J, Jadhav, K M, Bichile, G K, "Stuky of bulk magnetic properties of the mixed spinel $MgCr_xFe_{2-x}O_4$," Indian Journal of Pure & Applied Physics, 39,226 (2001).

Chapter-5

Results and Discussion

5.1 Characterization of $(Fe_{1-x}Mn_x)_{75}P_{15}C_{10}$

We have investigated in this thesis work, structural, transport and magnetic properties of double exchange $(Fe_{1-x}Mn_x)_{75}P_{15}C_{10}$ (x=0.00, 0.10, 0.20 and 0.30) amorphous ferromagnetic alloys.

5.1.1 Structural property

In order to check the structural property of $(Fe_{1-x}Mn_x)_{75}P_{15}C_{10}$, X-ray diffraction of as cast samples were taken with CuK_α (λ= 1.54178 Å) radiation by an X-ray diffractometer (model: PW 3040-X'Pert PRO Philips) at BAED . Fig.5.1 illustrates the X-ray diffraction patterns for all as cast samples within scanning angular range from 35° to 80°. From fig.5.1 we see that each sample contains a small broad peak which confirms that the samples are amorphous in nature.

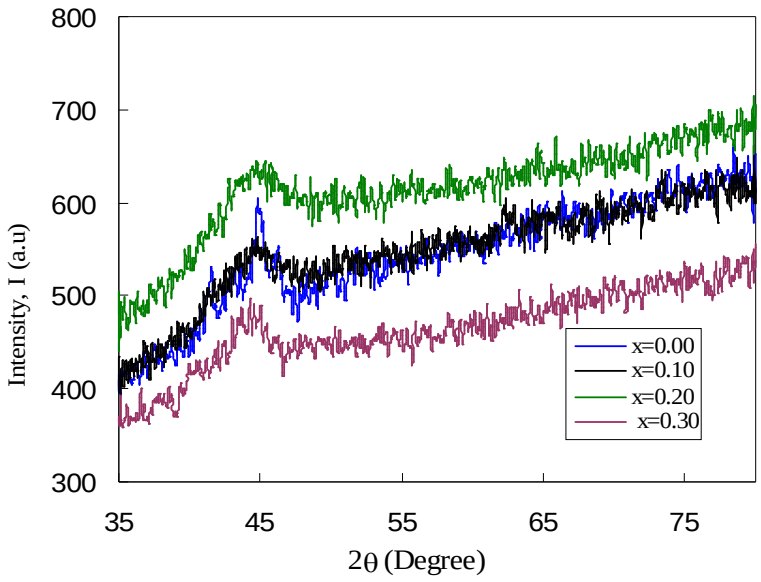

Figure 5.1: X-ray diffraction pattern of varies $(Fe_{1-x}Mn_x)_{75}P_{15}C_{10}$

5.2.1Transport properties measurement

Two important characteristics of the electrical resistivity of metallic glass are
(1) their resistivity is relatively high, greater than 1μΩm at room temperature
(2) their temperature coefficient of resistivity is very small and can be positive or negative. The combination of these two properties leads to a very high residual resistivity at 0K. The high resistivity of amorphous alloy compared with that of the same alloy in the crystalline state is related to the increased scattering of the conduction electrons due to a random atomic arrangement. In such a random structure, the phonon contribution to the scattering of electrons is small, hence the small temperature coefficient of resistivity. A single theory which not to be able to provide any quantitative description of the low temperature transport properties of the transition metal alloy. Moreover, there are no theoretical grounds for believing that there is common explanation for the anomalous behavior of the resistivity with respect to temperature because of complicated interplay between configuration, thermal and magnetic disorder [1].
The temperature dependence of the resistivity for amorphous alloys is well approximated as

$$\rho = \left[\rho_0 + \delta\rho(T)\right]\exp[-2W(T)] \tag{5.1}$$

$$W(T) = W(0)(\frac{T}{\Theta_D}) + ... \tag{5.2}$$

$$W(0) = 3\frac{(\hbar K)^2}{8\mathrm{M}K_B\Theta_D} \tag{5.3}$$

where, D (w) is the phonon density of the states per atom. ρ_0 is the residual resistivity, $\Delta\rho(T)$ is the term arising from the inelastic eletron- phonon interaction and the exponential term $\exp[-2W(T)]$ represents the Debye –Wallar factor . The term $\Delta\rho(T)$ is shown to exhibit $+T^2$ dependence at low temperatures and +T at higher temperatures. The Debye -Wallar factor yields $(1-\alpha T^2)$ dependence at low temperature and the (1-ßT) above about several tens of degrees K. The quantity α and ß are the temperature coefficient of resistivity factors at low and high temperature respectively. The validity of equation (5.1) has been experimentally confirmed by Mizutani [2] for amorphous alloys.

5.2.2 Room Temperature Resistivity

Isotropic and anisotropic spin scattering mechanisms should contribute to the resistivity in magnetically ordered amorphous metals [3-7]. For the scattering centers magnons, magnetic impurities and topological spin disorder have been proposed [3, 7, and 8]. In some cases, the structural disorder of the atomic sites introducing magnetic scattering to the resistivity [3, 9]. Fig.5.2 shows the room temperature resistivity of $(Fe_{1-x}Mn_x)_{75}P_{15}C_{10.}$ Resistivity of the examine samples increases with the increase of Mn content. According to the previous report of "some thermal properties of amorphous $(Fe_{1-x}Mn_x)_{75}P_{15}C_{10}$ ribbons"[13], if we increase Mn content in the system the magnetic impurities, scattering and topological spin disorder are thought to be responsible for the increase of resistivity.

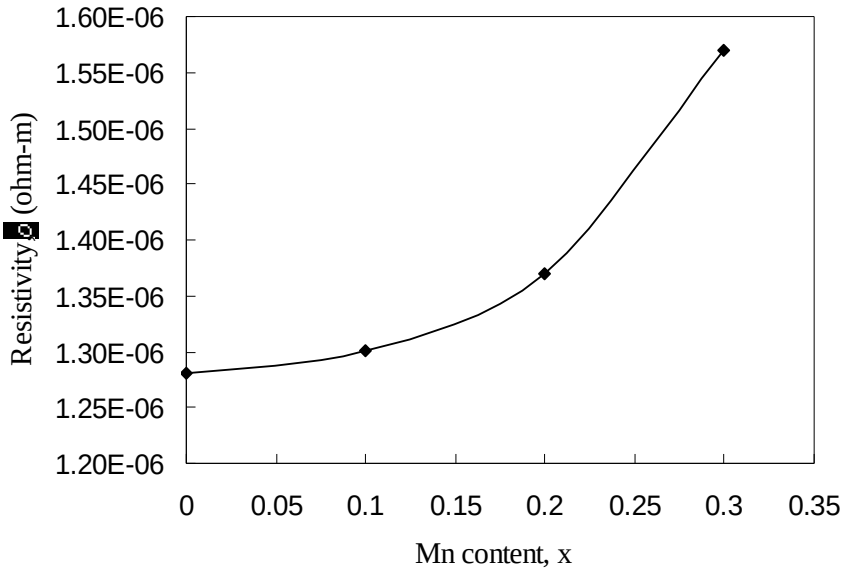

Figure 5.2: Room temperature resistivity of varies $(Fe_{1-x}Mn_x)_{75}P_{15}C_{10}$

Table 5.1: Room temperature (298K) resistivity of varies $(Fe_{1-x}Mn_x)_{75}P_{15}C$

Sample	ρ_0 (ohm-m)	ρ_0 (ohm-m), Ref. [9]
x=0.00	1.28×10^{-6}	1.513×10^{-6}
x=0.10	1.32×10^{-6}	1.607×10^{-6}
x=0.20	1.37×10^{-6}	1.730×10^{-6}
x=0.30	1.57×10^{-6}	1.825×10^{-6}

5.2.3 Temperature dependent Resistivity

Fig.5.3 shows the temperature dependent resistivity of varies $(Fe_{1-x}Mn_x)_{75}P_{15}C_{10}$. Resistivity decreases almost linearly with the decreases in temperature for sample, x=0.00. In this case there is no contribution of Mn, the decrease in resistivity with decrease in temperature may be assumed that the incoherent electron-magnon scattering decreases. But for x=0.30 resistivity decreases upto Curie temperature (T_c) and also the resistivity shallow minima observed which has been assigned to a competition of structural and spin scattering [11]. Spin scattering is maximal at T_c and then stay constant [12]. Thus the rises of ρ (T) occur above and below T_c suggesting that there have two conductivity regimes. The Curie temperature (T_c) of x= 0.30 is 166K [13]. Resistivity increases above and blow this Curie temperature is due to structural topological scattering. In the case of x=0.10 and x=0.20 the resistivity increases with the decrease in temperature. Since the Curie temperature (T_c) of x =0.10 is 420K and x=0.20 is 350K [13] respectively. Thus the resistivity increases below the Curie temperature is due to the structural topological scattering. The temperature coefficient of resistivity (TCR) is negative below the Curie temperature for samples x=0.10, 0.20, 0.30 and (TCR) is positive for sample x=0.0. The diffraction model says that in the case of metallic glasses ρ (T) will be straight line in the temperature range $120K \leq T \geq 300K$ and in the region $50K \leq T \geq 100K$, ρ (T) would be follow T^2 law. These two conditions are consistence with our resistivity results.

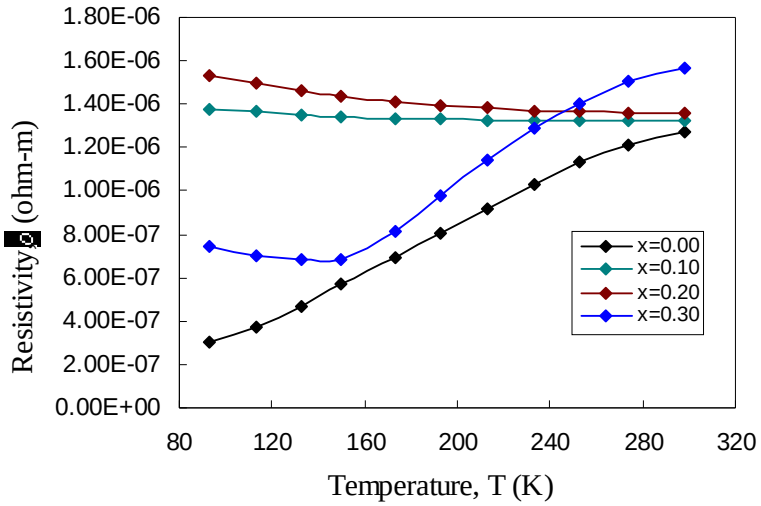

Figure 5.3: Temperature dependent resistivity of $(Fe_{1-x}Mn_x)_{75}P_{15}C_{10}$

Table 5.2: Resistivity at room temperature ρ_0 and temperature coefficients of the resistivity α in the range of 110K<T<273K.

Sample x	ρ_0 (10^{-6} Ω-m)	T (K)	α_o (10^{-10} μΩ-m/k) (114-273)K
0.00	1.28	298	54
0.10	1.31	298	-3.8
0.20	1.35	298	-8.22
0.30	1.57	298	-62

From table 5.2 we see that temperature coefficient of resistivity is very small. Since metallic glass is random atomic structure arrangement. In such a random structure, the phonon contribution to the scattering of electrons is small, hence the small temperature coefficient of resistivity

5.2.4 Normalized Resistivity

Fig.5.4 shows the normalized resistivity versus temperature for $(Fe_{1-x}Mn_x)_{75}P_{15}C_{10}$. From the suppressed scale one reads that ρ increases for x=0.10, 0.20, 0.30 below the Curie temperature and decreases for x=0.00 which one generally expect for this amorphous alloys [10]. In the case of x=0.30 we find a minimum in ρ which indicating that there is a magnetic contribution to the scattering process.

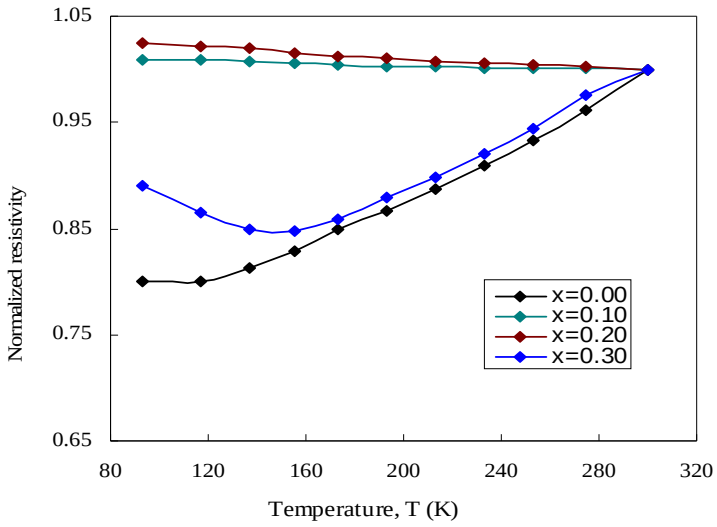

Figure 5.4: Normalized resistivity of varies $(Fe_{1-x}Mn_x)_{75}P_{15}C_{10}$

5.2.5 Hall resistivity

The Hall effect measurement is carried out using the configuration shown in fig. 4.4. An electrical current is feed along the x direction in a rectangular specimen and a magnetic field is applied to the z direction. Since no current flows along the y and z directions, the condition $J_x = J_y = 0$ holds. The transverse electric field E_y is developed along the y direction. The Hall coefficient R_H and Hall Resistivity, ρ_H were calculated using equations (4.5) and (4.6) respectively. Fig 5.5 shows the Hall resistivity of $(Fe_{1-x}Mn_x)_{75}P_{15}C_{10}$ alloys as a function of magnetic field applied along the z-direction. It is seen that the Hall resistivity initially increases very rapidly. Once saturation is achieved and there is no domain motion as it has assumed a single domain. For crystalline materials the origin of the Hall voltage is superimposed on that due to the free carriers if magnetic order is present [14]. One must consider the quantum mechanical side jump mechanism [9, 15] according to which the electrons a small transverse deflection at each scattering event. If this mechanism were dominant in our alloys p_H should be proportional to ρ^2. One or more of the scattering processes, impurity, phonon and spin disorder scattering give dominant contribution to the anomalous Hall effect.

The non linear behavior of the $\rho_H \sim \mu_0 H$ curve decomposed into the normal Hall effect due to the lorentz force and a strongly depend on the magnetization component and is explicitly written as

$$\rho_H = R_0 \mu_0 H + R_s M_s$$

The first term, characterized by the ordinary Hall coefficient R_0, is the contribution from the ordinary Hall effect for the Lorentz force. The second term characterized by the extraordinary or anomalous Hall coefficient R_s, represents a strongly dependent on the magnetization of the materials.

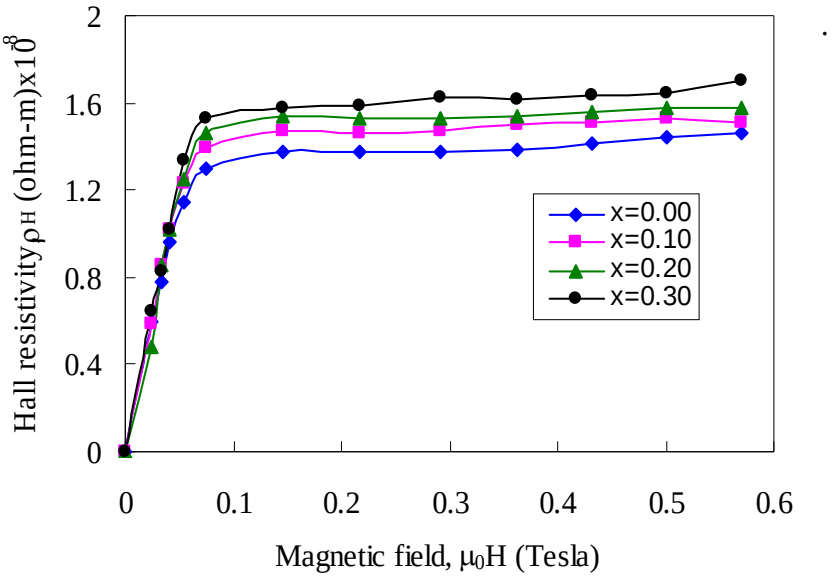

Figure 5.5: Hall resistivity vs Magnetic field of $(Fe_{1-x}Mn_x)_{75}P_{15}C_{10}$

From figure 5.6 we see that Hall coefficient increases with the increase of Mn concentration and it is sharply increases upto a certain magnetic field after that R_H exponentially decreases with the increase applied magnetic field. Thus the value of the Hall coefficient depends on the type, number, impurity, spin disorder and properties of the charge carriers that constitute the current.

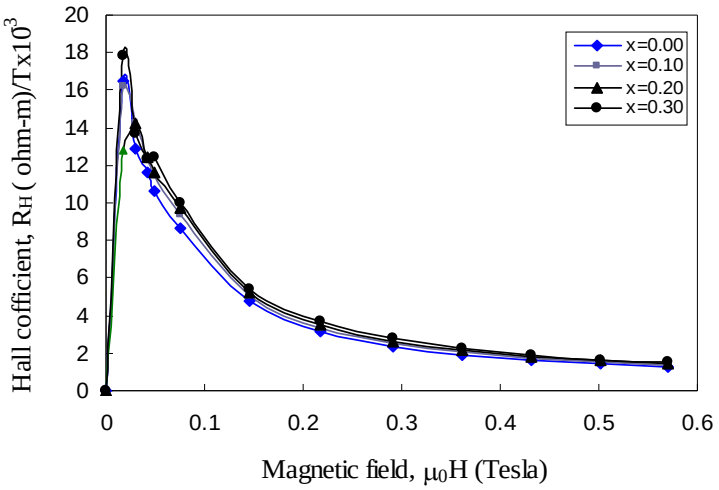

Figure-5.6: Hall coefficient vs Magnetic field of $(Fe_{1-x}Mn_x)_{75}P_{15}C_{10}$

.

5.2.6 Magnetoresistance Measurement

The magnetoresistance of the samples were calculated using the following formula

$$MR\% = \frac{R(H) - R(0)}{R(0)} \times 100\%$$

where, R(H) is the resistance in presence of magnetic field and R(0) is the resistance in absence of magnetic field. The magnetoresistance measurement was carried out by measuring current, applied magnetic field and the developing voltage. The magnetic field is applied to the perpendicular of current. The magnetoresistance measurement can disclose the presence or absent of preferred domain orientations in the demagnetized state. The physical origin of the magnetoresistance effect lies in spin orbit coupling. As M rotates, the electron cloud about each nucleus deforms slightly and this deformation changes the amount of scattering undergone by the conduction electrons in their passage through the lattice. During the demagnetization process the magnetic domains and the conduction electron scatterings take part to contribute to the electrical resistivity and the magnetoresistance. Fig-5.7 shows the MR% at room temperature for different manganese (Mn) concentrations. It is seen from the figure that MR% increases with increase of manganese concentration. According to the previous report if Mn concentration increase in the system topological spin disorder

increases and hence MR% increases with Mn concentration. An initial large change in resistivity is accompanied by growth of magnetic domain parallel to the direction of the magnetic field. Once the magnetic saturation is achieved there is no domain motion as it has assumed a single domain. The only contribution to the electrical resistivity and the magnetoresistance comes at this stage is from the conduction electron scattering due to the collision between themselves and the electron mean free-path is much longer in this stage. The MR% varies from 0 to 6% with the variation of Mn content.

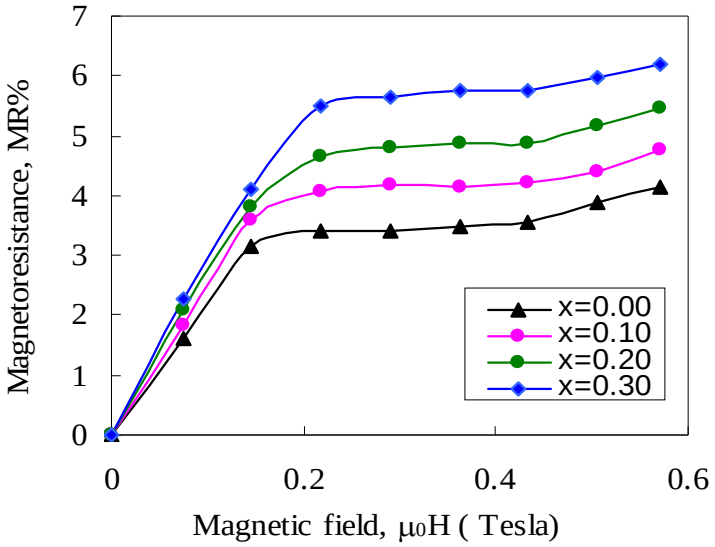

Figure 5.7: Variation of Magnetoresistance varies of $(Fe_{1-x}Mn_x)_{75}P_{15}C_{10}$

5.3 DTA, TGA, DTG Analysis

Figure 5.9(a-d) shows the differential thermal analysis (DTA), thermo-gravimetric analysis (TGA) and differential thermo-gravimetric (DTG) of the ribbons. The heating rate was 20°C/min.

DTA: In the DTA curve only one exothermic peak rises occurred for each sample. The peak of each sample is attributed to the crystallization temperature. Crystallization temperature increases with increase of Mn content in the $(Fe_{1-x}Mn_x)_{75}P_{15}C_{10}$ system which is shown in fig.5.8. Crystallization temperature of different samples is also given in table 5.3

Table-5.3: DTA peak values of different $(Fe_{1-x}Mn_x)_{75}P_{15}C_{10}$ samples

Samples	Peak (°C)
x=0.00	419
x=0.10	436
x=0.20	439
x=0.30	472

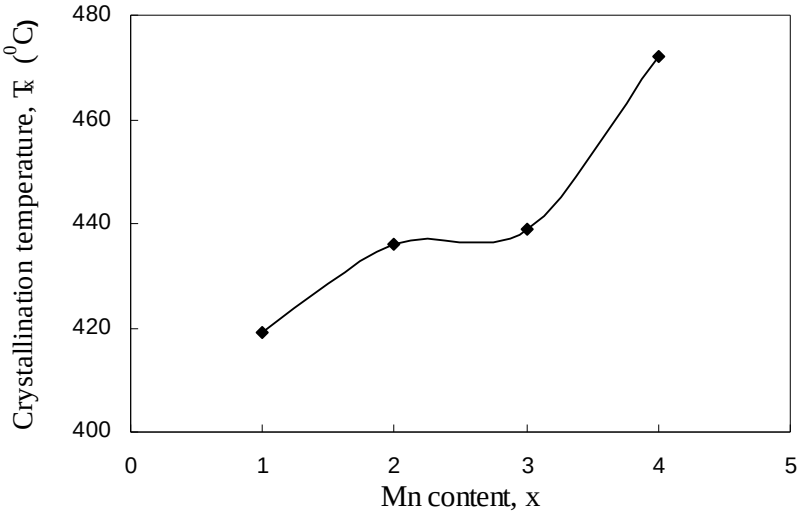

Figure 5.8: DTA peak values varies with Mn content

TGA %: In TGA % vs T curve we observed that mass is slightly gained in all samples. As temperature is increased the micro voids which formed during the growth process of the ribbons during melts spinning is gradually eliminated. This results in densification of the matrix of the more ordered crystallites in the samples at higher temperature. At higher temperature Fe and Mn ions absorb "O" from the experimental environment and hence mass are slightly gained at higher temperature. Gained of the mass increases with the increase of Mn concentration into the $(Fe_{1-x}Mn_x)_{75}P_{15}C_{10}$ because the ionic radius of Mn (0.89 Á) is larger than the ionic radius of Fe (0.74 Á).

DTG: In DTG% vs T curves we see that some small peaks are found for samples x=0.0 and 0.20 which means that there is a small change of mass with a small

difference heating temperature. But for x=0.10 and 0.30 some broad peaks are found which indicating that there is large change of mass occur within small difference of the heating temperature

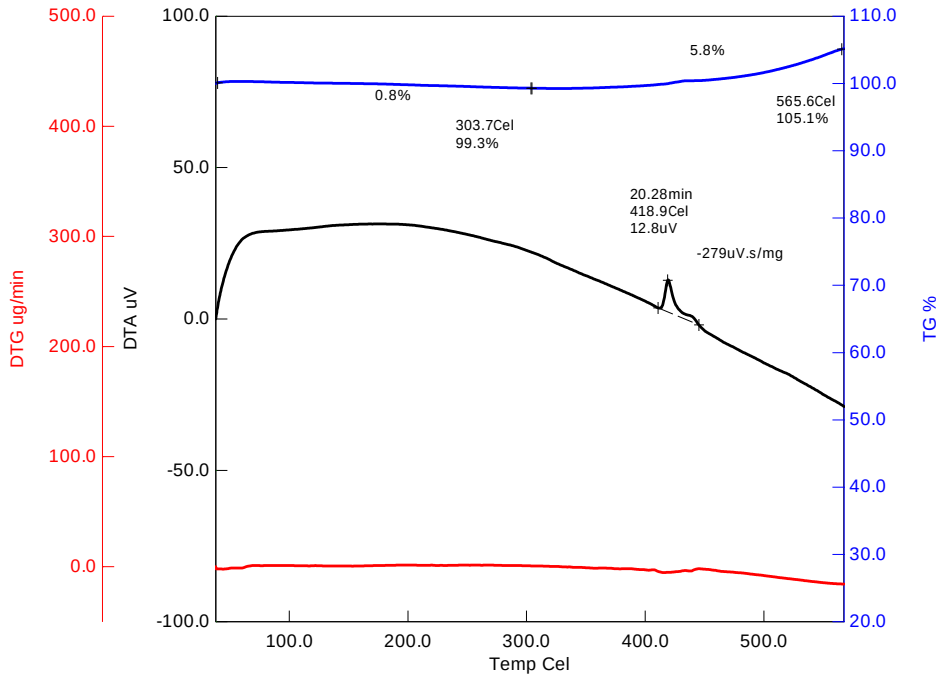

Figure 5.9 (a): DTA, TGA, DTG curve for sample, x=0.00

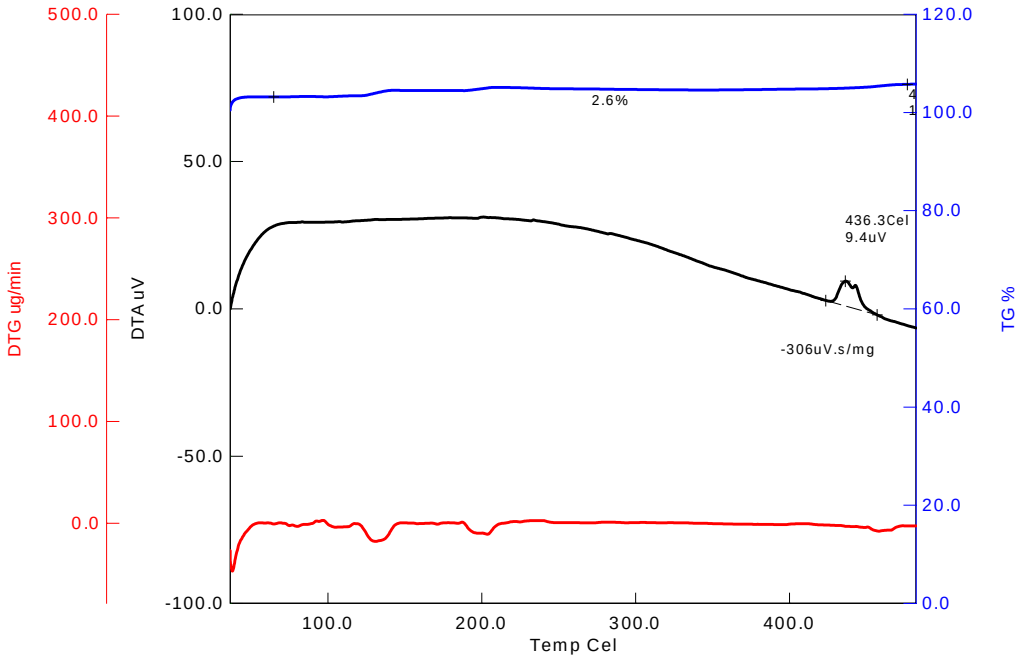

Figure 5.9 (b): DTA, TGA, DTG curve for sample, x=0.10

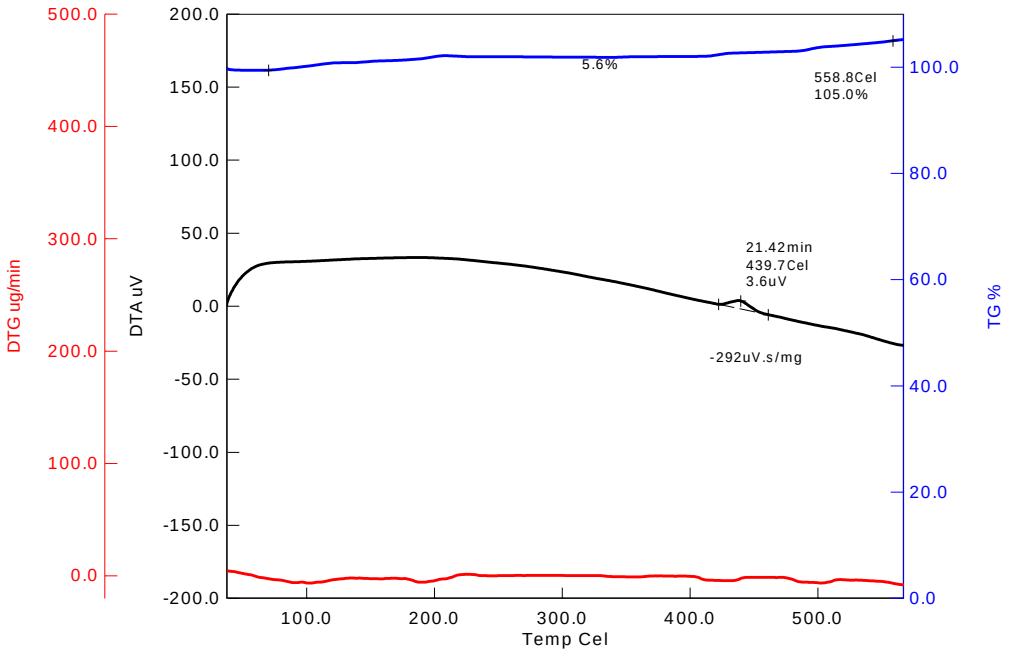

Figure 5.9 (c): DTA, TGA, DTG curve for sample, x=0.20

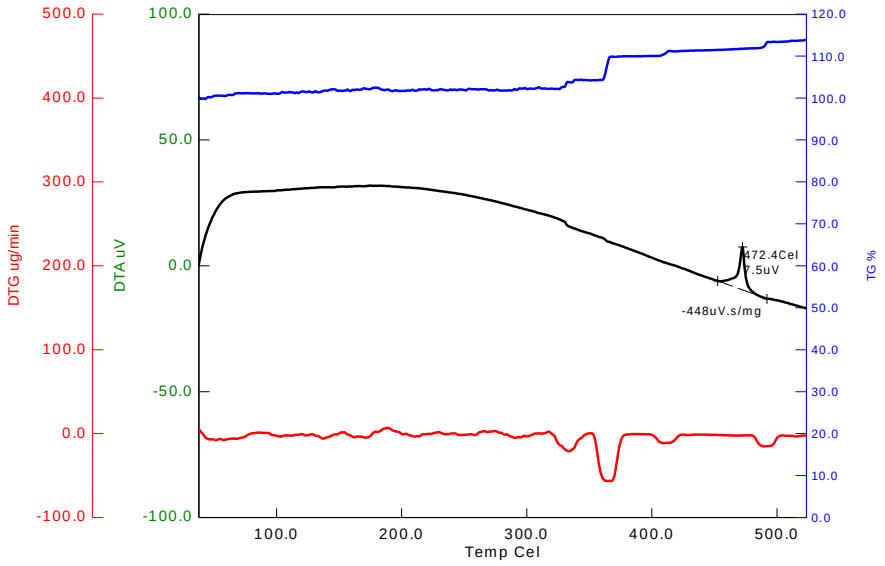

Figure 5.9 (d): DTA, TGA, DTG curve for sample, x=0.30

5.4 Magnetization Measurement

The magnetization of the samples was determined with the help of Vibrating Sample Magnetometer. We have calibrated the VSM using a 152mg spherical sample of 99.99% pure nickel of known saturation magnetic moment. The current was applied to the electromagnet by Agilent power supply upto 8 ampere and the corresponding magnetic field was measured by the Gauss meter. The ratio transformer reading was recorded and the actual calibration of the VSM was determined from the relation (4.9) and the magnetization of the ribbons samples were calculated using the following eq^{n}

$$M = \frac{KV}{m} \text{ emu/g} \qquad (5.2)$$

where, M= Magnetization

m= Mass of the experimental sample

V= Voltage correspond to the magnetization

K= Calibration constant of the VSM

The relation between the saturation magnetization, M_s at 0°K and the number of Bohr magnetrons, n_B per molecule is

$$n_B = \frac{M}{5585} \times Ms \qquad (5.3)$$

Where, M is the molecular weight of the substance.

Magnetization measurements of $(Fe_{1-x}Mn_x)_{75}P_{15}C_{10}$ amorphous alloys represented in fig 5.10. From figs. 5.10 and 5.11 we see that the saturation magnetization decreases with the increase of Mn content into the $(Fe_{1-x}Mn_x)_{75}P_{15}C_{10}$ system. Saturation magnetization is related to the average magnetic moment per formula $(Fe_{1-x}Mn_x)_{75}P_{15}C_{10}$ unit. Since the saturation magnetization decreases the average magnetic moment per formula unit decreases according to equation (5.3). If Mn content increases in the system isolated AF- coupled sites simply order antiparallel to the majority FM order. This means that the antiferromgnetic interactions introduced by Mn atoms cause deviations from a pure ferromagnetic structure also at low Mn concentration and hence the total magnetization and the average magnetic moment per formula unit of $(Fe_{1-x}Mn_x)_{75}P_{15}C_{10}$ decreases with the increase of Mn content [16].

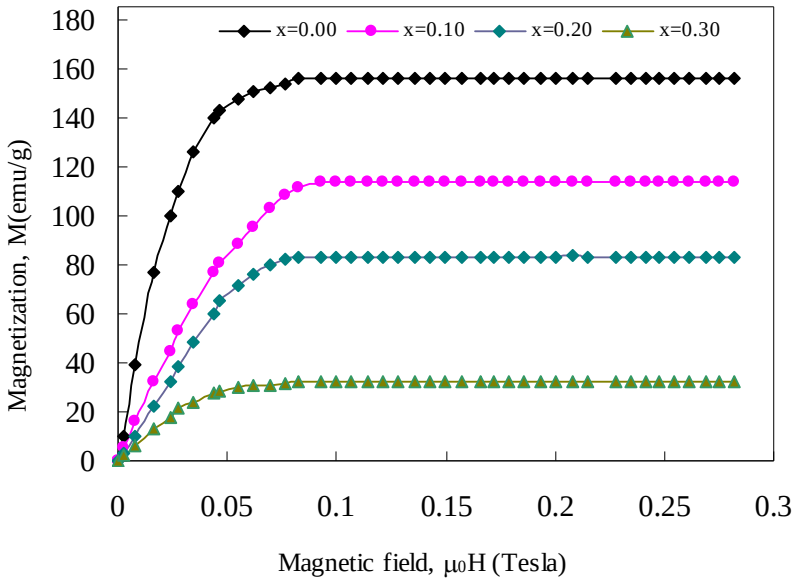

Figure 5.10: Variation of magnetization of $(Fe_{1-x}Mn_x)_{75}P_{15}C_1$ with Mn and applied magnetic field

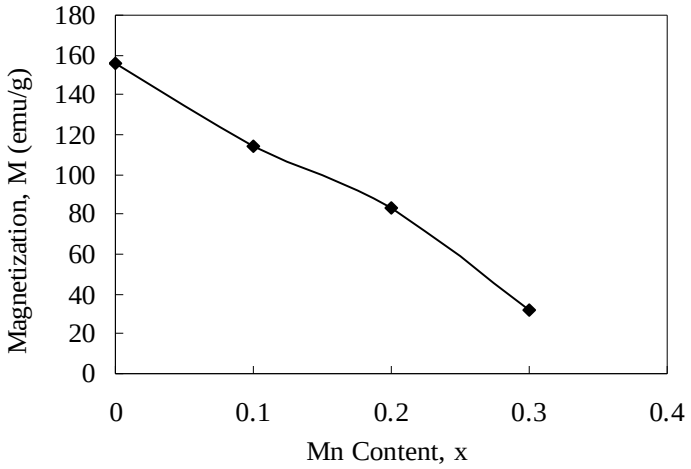

Figure.5.11: Variation of saturation magnetization of $(Fe_{1-x}Mn_x)_{75}P_{15}C_{10}$ with Mn content

Table-5.4: Data for Saturation Magnetization

Samples	Saturation Magnetization , Ms (emu/g	Bohr Magneton per formula unit
x=0.00	155	1.33
x=0.10	114	0.97
x=0.20	83	0.71
x=0.30	32	0.23

5.5 Permeability Measurement

5.5.1 Complex permeability

The dynamic response of the magnetic domains to the external magnetic field determines the complex permeability. The value of complex permeability provides the information about the inertia of the domains, their distribution and mutual coupling. The phase lag between the applied field and the response of magnetic domains determine the real, $\mu^{/}$ and imaginary, $\mu^{//}$ parts of the complex permeability. The studied sample is obtained by a quenching method with nominal composition of $(Fe_{1-x}Mn_x)_{75}P_{15}C_{10}$. Since this sample is as prepared, so its grains size is assumed to be uniform.

The complex permeability is related into two mechanisms; one is the domain wall movement, which dependents on the grain size and the other is spin rotation as reported by A. Paduraru et al [17].

The real and imaginary parts of the complex permeability were measured as a function of frequency ranges from 100Hz to 100 MHz for as cast samples. The measured technique was based on the determination of complex impedance of a loaded circuit with a toroidal-shaped samples using LF Impedance Analyzer [4192A, 5Hz- 110 MHz] at BCSIR.

The real, $\mu^{/}$ and imaginary, $\mu^{//}$, parts of complex permeability for as cast samples are presented separately as a function of frequency in figures-5.12 and 5.13.

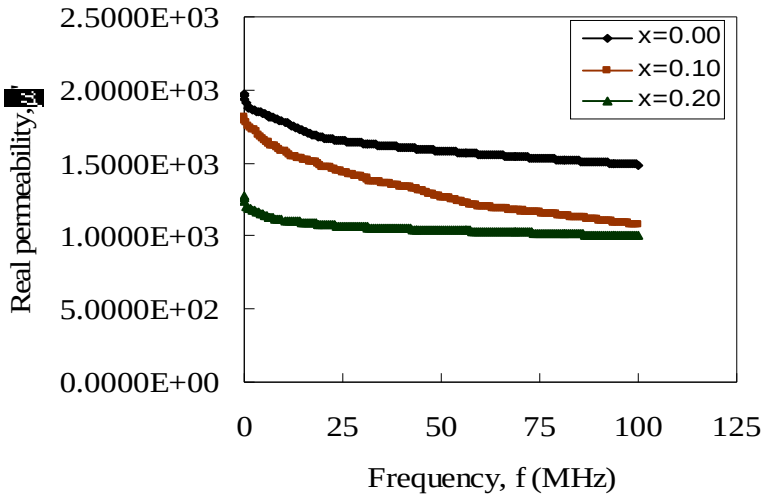

Figure.5.12: Variation of real permeability of $(Fe_{1-x}Mn_x)_{75}P_{15}C_{10}$ with frequency

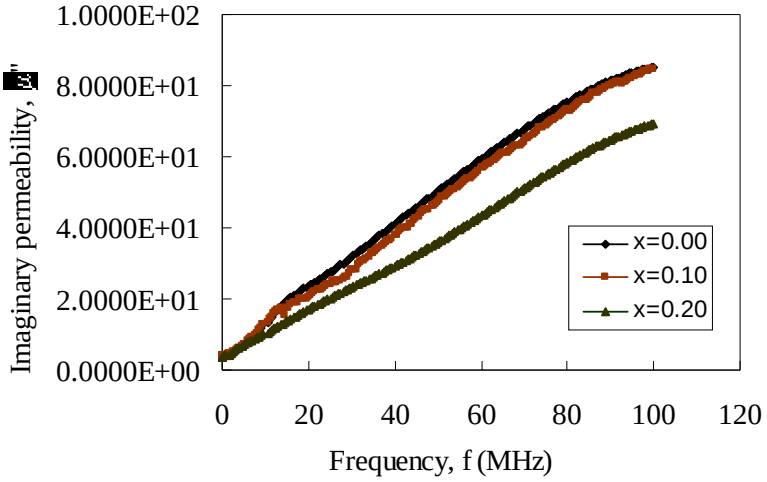

Figure 5.13: Variation of imaginary permeability of $(Fe_{1-x}Mn_x)_{75}P_{15}C_{10}$ with frequency

The real permeability decreases with the increase of Mn content as shown in fig. 5.14 and also with the frequency. Imaginary permeability increases linearly with the increase in frequency which means that at higher frequency domains do not follow the applied field.

At low frequency permeability originating from the Bloch wall motion since the permeability does not drop to zero, the permeability originating from BW-motion is not very high, i.e. the BW's are not very mobile from the start. That in turn suggests very broad BW's. When the frequency gets higher, the BW cannot follow the applied

force. But the Bloch wall oscillations could yield a very strong oscillator with a high loss developing near to the BW-motion regime.

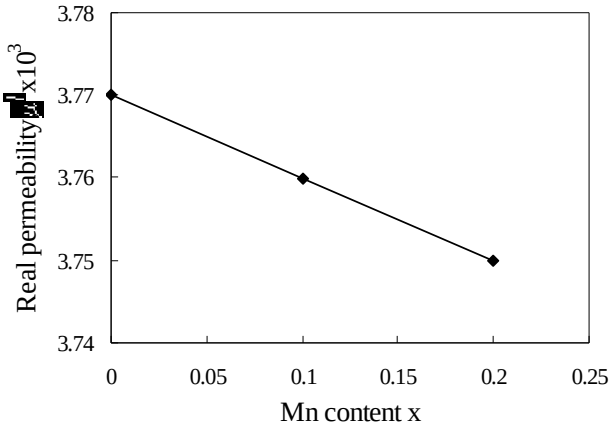

Figure 5.14: Decrease of real permeability with Mn content

References

1. Brouers, F. and Brauwers, M., "On the temperature dependence of electrical resistivity in concentrated disorder transition binary alloys", J.Phys.Paris 36, L17-21 (1975)

2. Mizutani, U. "The magnetism of amorphous metals and alloys", Prog. Mat. Sci. 28, 97 (1983)

3. Heinemann, K., and Barner, K., "Magnetic field sensor for cryog enic applications",J. Appl.Phys.Lett. 50,1284 (1987)

4. Cote, P.J. and Meisel, L.V., Glassy Metals I, eds.H.-J. Guntherrodt and H. Beck (Spinger Verlag, Berlin, p.141 (1981)

5. Sinha, A.K., "Temperature and Field Dependence of Magnetization of Amorphous (Fe, Mn)-P-C Alloys", J.Appl. Phys. 42, 338 (1971)

6. Heinemann, K. Ph.D. thesis**,** University of Göttingen, Germany, (1987)

7. Kaul, S.N., Kettlerr, W.and Rosenberg, M. "Evidence for a magnetic contribution to the electrical resistivity in amorphous $Fe_{80}B_{20-x}C_x$ alloys", Phys Revs.B33 p4987(1986)

8. Kaul, S.N., "Anomalous Hall effect in nickel and nickel- rich nickel-copper alloys",Phys. Rev.B 20 ,5122 (1979)

9. Erle, A. and Barner, K., "High pressure resistivity of MnAs" J. Magn.Mat. 74 (1988)

10. Heinemann, K., and Bärner**,** K., "Transport and magnetic properties of amorphous $(Fe_{1-x}Mn_x)_{75}P_{15}C_{10}$ alloys" J. Magn. Magn. Mater., 80, 257-264 (1989)

11. Barner, K., Schunemann, J-W., Heinemann, K., A.A. Ganin, Bersenev, Yu. S. and Medvedeva, I.V.,IC Physics of Transition Metals Darmstadt V.II. Ed.'s P.M. Oppneer, J.Kubler World Scientific , Singaporep698 (1993)

12. Heinrich, B., Fraitova, D., Kambersky, V., "The Influence of s-d Exchange on Relaxation of Magnons in Metals", Phys. Stat. Sol, (b)23, 501 – 507 (2006)

13. Kraus, E., Barner, K., Heinemann, K., Kanomata, T., Medvedeva, I.V., Maldal, P., and Gmelin, E., "Some thermal properties of amorphous $(Fe_{1-x}Mn_x)_{75}P_{15}C_{10}$ Ribbons" , Phys. Stat. Sol (a) 157, 449 (1996

14. Hurd, C.M., "The Hall effect in Metals and Alloys" (Plenum Press, new York, 1972)

15. Berger, L., "Side –jump mechanism for the Hall effect of ferromagnets" Phys. Rev.B 2, 4559 (1970)

16. Ryan, D. H., Beath, A. D., and McCalla, E., “Transverse spin freezing in α – (Fe1-xMn)78Si8B14: A site frustrated metallic glass” Phys. Rev. B 67, 104404 (2003)
17. Paduraru, A., Kenoufi A., Bailey, N. P., Schiotz, J., “An Interatomic Potential for Studying CuZr Bulk Metallic Glasses”, Advanced Engineering Materials, 9, 505 – 508 (2007)

Chapter-6

Conclusions and Future Work

6.1 Conclusions

The melt spinning technique have been described in this study to obtain amorphous $(Fe_{1-x}Mn_x)_{75}P_{15}C_{10}$ ribbons. The effects of varying the composition, structural, transport and magnetic properties were studied of the prepared samples. The results of the present work are summarized and the following conclusive statements can be made from this research work.

The X-ray diffraction patterns show that each sample contains a small broad peak which confirms the samples are amorphous in nature.

Room temperature resistivity increases with the increase of Mn content in the system. Resistivity decreases with decrease in temperature for sample, x=0.00. Since there is no contribution of Mn, the decrease in resistivity is assumed that the incoherent electron-magnon scattering decreases with the decrease in temperature. Resistivity increases below the Curie temperature for samples x=0.10 and x=0.20. But for x=0.30 resistivity decreases, upto Curie temperature and then resistivity increases with decreases in temperature. Increase of resistivity above and blow the Curie temperature is due to structural topological scattering.

The Hall resistivity has shown sharp increase initially with magnetic field. Once saturation is achieved, there is no domain motion as it has assumed a single domain. Hall resistivity increases with increasing of Mn concentration and also the applied magnetic field. If we increase Mn, magnetic impurities and topological spin disorder increases which may be responsible for the increases of Hall resistivity with Mn. One or more of the scattering processes impurity, phonon and spin disorder scattering give dominant contribution to the anomalous Hall effect in different filed which, in turn, are different for different samples

The Magnetoresistance (MR%) initial large change occur in the low field which is accompanied by growth of magnetic domain parallel to the direction of the magnetic field. Once the magnetic saturation is achieved there is no domain motion as it has assumed a single domain. The only contribution to the electrical resistivity and the magnetoresistance comes at this stage is from the conduction electron scattering due to the collision between themselves and the electron mean free-path is much longer in this stage. The MR% varies from 0 to 6% with the increase of Mn content.

In DTA curve only one exothermic peak arises occurred for each sample. The peak values increases with increase in Mn concentration. Theses Peaks are attributed to the crystallization temperature.

In TGA % curve we see that as the temperature is increased the micro voids which formed during the growth process of the ribbons during melts spinning is gradually eliminated. This results in densification of the matrix of the more ordered crystallites in the samples at higher temperature. At higher temperature Fe and Mn ions absorb O from the experimental environment and hence mass are slightly gained at higher temperature. Mass gained increases with the increase of Mn concentration into the $(Fe_{1-x}Mn_x)_{75}P_{15}C_{10}$

Magnetization of $(Fe_{1-x}Mn_x)_{75}P_{15}C_{10}$ decreases with increase of Mn content. If we increase Mn, isolated AF interaction introducing increases with the majority FM order.Thus the antiferromagnetic interactions introduced by Mn atoms cause deviations from a pure ferromagnetic structure at low Mn concentration and hence total magnetization and the average magnetic moment per formula unit of $(Fe_{1-x}Mn_x)_{75}P_{15}C_{10}$ decreases with the increase of Mn content.

The real permeability decreases with the increase of Mn content and also with the frequency. Imaginary permeability increases with the frequency which means that at higher frequency domain does not follow the applied field.

$(Fe_{1-x}Mn_x)_{75}P_{15}C_{10}$ alloys have shown soft magnetic properties. This alloy can be very useful material for manufacturing different kinds of switching devices. The alloy has shown superior magnetic and electrical properties which can be very useful in selecting the domain within which the devices can work to serve some specific purpose for its application. This alloy can also work in other magnetic phases and is specialized application.

6.2 Suggestions for future work

The following experiments can be carried out for understanding the magneto-transport and the structural properties of $(Fe_{1-x}Mn_x)_{75}P_{15}C_{10}$

1. Temperature dependent magnetic a.c. permeability and magnetization may be measured to determine the Curie temperature (T_c).
2. Neutron scattering can be done to identify the magnetic structure
3. Field cool (FZ) and zero field cool (ZFC) experiment would be performed
4. Magnetic anisotropic constant measurement
5. Spin wave resonance justify experiment
6. Structure can be done with high resolution of SEM .

List of Symbols and Nomenclature

A	-	Stiffness Constant
Fe	-	Iron
Cu	-	Copper
Nb	-	Niobium
Ta	-	Tantalum
Si	-	Silicon
B	-	Boron
Co	-	Cobalt
Mn	-	manganese
C	-	Carbon
P	-	Phosphorus
$\rho(0)$	-	Resistivity at room temperature.
$\rho(T)$	-	Resistivity at any temperature (other than room temperature)
$\frac{\rho(T)}{\rho(0)}$	-	Normalized resistivity
$\frac{\Delta\rho}{\rho(0)}$	-	Magnetoresistance
$\frac{\Delta\rho}{\rho}$	-	Reduced resistivity
MR%	-	Magnetoresistance in percent.
δ	-	Wall width
MI	-	Magnetoimpedance
GMR	-	Giant Magnetoresistance
GMI	-	Giant magnetoimpedance
R	-	Resistance
X	-	Reactance
QF	-	Quality factor
DF	-	Dissipation factor
L	-	Inductance
L_{ex}	-	Exchange interaction length

μ_0	-	Permeability in free space.
μ_i	-	Initial permeability
μ'	-	Real part of complex permeability
μ''	-	Imaginary part of complex permeability
H_c	-	Coercivity
E_k	-	Anisotropy energy
Ms	-	Saturation magnetization
D	-	Grain diameter
T_C	-	Curie temperature
T_G	-	Glass transition temperature
KG	-	Kilogauss
MHz	-	Megahertz
GHz	-	Gigahertz
AHE	-	Anomalous Hall effect
SWR	-	Spin wave resonance
FM	-	Ferromagnetic
AFM	-	Anti-ferromagnetic
FMR	-	Ferromagnetic resonance
WB	-	Bloch wall
DTA	-	Differential Thermal Analysis
TGA	-	Thermogravometric Analysis
DTG	-	Differential Thermal Gravimetric

APPENDIX

Table-1: Room temperature (298K) resistivity

A. Sample: $(Fe_{1-x}Mn_x)_{75}P_{15}C_{10}$ [x=0.00, 0.10, 0.20 and 0.30]

B. Sample Size:

Length: $l=1.2x10^{-2}$ m.
Width: $w= 8 \times 10^{-4}$ m
Thickness: $t= 25 \times 10^{-6}$ m

Magnetic field, H (T)	Resistivity, ρ(ohm-m)x10^{-6} x=0.00	Resistivity, ρ(ohm-m) x10^{-6} x=0.10	Resistivity, ρ(ohm-m) x10^{-6} x=0.20	Resistivity, ρ(ohm-m) x10^{-6} x=0.30
0	1.27163	1.3214	1.3562	1.5665
0.0748	1.2889	1.402563	1.43351	1.60187
0.1453	1.4111	1.46724	1.47941	1.631
0.2175	1.3048	1.47123	1.47941	1.67204
0.291	1.37827	1.503124	1.53802	1.62655
0.362	1.2881	1.52231	1.54446	1.66928
0.432	1.26536	1.482365	1.56186	1.67904
0.501	1.36015	1.46562	1.544927	1.65413
0.57	1.39645	1.4423156	1.544592	1.68405

Table-2: Temperature (93-298) K dependence resistivity

A. Sample: $(Fe_{1-x}Mn_x)_{75}P_{15}C_{10}$ [x=0.00, 0.10, 0.20 and 0.30]

B. Sample Size:
Length: $l=1.2x10^{-2}$ m.
Width: $w= 8 \times 10^{-4}$ m
Thickness: $t= 25 \times 10^{-6}$ m

Temperature, T(K)	Resistivity, ρ(ohm-m) x10^{-6} x=0.00	Resistivity, ρ(ohm-m) x10^{-6} x=0.10	Resistivity, ρ(ohm-m) x10^{-6} x=0.20	Resistivity, ρ(ohm-m) x10^{-6} x=0.30
298	1.27163	1.3214	1.3562	1.5665
273	1.211989	1.321796	1.358641	1.527338
253	1.131417	1.322457	1.363668	1.432643
233	1.028458	1.323648	1.371441	1.319464
213	0.919442	1.326162	1.382275	1.183559
193	0.804511	1.329876	1.395822	1.036798
173	0.688662	1.335727	1.412572	0.884388
153	0.574344	1.343474	1.43489	0.734042

133	0.466942	1.353685	1.463588	0.619532
113	0.373553	1.365191	1.495055	0.557579
93	0.29879	1.377887	1.531385	0.540918

Table-3: Normalized resistivity (ρ/ρ_0) for temperature (93-298) K

A. Sample: $(Fe_{1-x}Mn_x)_{75}P_{15}C_{10}$ [x=0.00, 0.10, 0.20 and 0.30]

B.Sample Size:

Length: $l=1.2x10^{-2}$ m.

Width: $w= 8 \times 10^{-4}$ m

Thickness: $t= 25 \times 10^{-6}$ m

Temperature, T (K)	ρ/ρ_0 (x=0.00)	ρ/ρ_0 (x=0.10)	ρ/ρ_0 (x=0.20)	ρ/ρ_0 (x=0.30)
298	1	1	1	1
273	0.953	1.0003	1.0018	0.975
253	0.933	1.0005	1.0037	0.938
233	0.909	1.0009	1.0057	0.921
213	0.894	1.0019	1.0079	0.897
193	0.875	1.0028	1.0098	0.876
173	0.856	1.0044	1.012	0.853
153	0.834	1.0058	1.0158	0.830
133	0.813	1.0076	1.02	0.844
113	0.8124	1.0085	1.0215	0.900
93	0.799	1.0093	1.020	0.970

Table-4.: Hall coefficient measurement at room temperature

A. Sample: $(Fe_{1-x}Mn_x)_{75}P_{15}C_{10}$

B. Sample Size:

Length: $l=1.2x10^{-2}$ m.

Width: $w= 8 \times 10^{-4}$ m

Thickness: $t= 25 \times 10^{-6}$ m

Magnetic Field, H (Tesla)	Hall coefficient, R_H (Ohm-m)/T $x10^{-3}$, x=0.00	Hall coefficient, R_H (Ohm-m)/T $x10^{-3}$, x=0.10	Hall coefficient, R_H (Ohm-m)/T $x10^{-3}$, x=0.20	Hall coefficient, R_H (Ohm-m)/T $x10^{-3}$, x=0.30
0	0	0	0	0
0.018	16.48333	16.25556	12.77777778	17.84167
0.03	12.92167	14.20517	14.27166667	13.72667

0.0413	11.66102	12.38499	12.38983051	12.38499
0.05	10.62037	11.43519	11.60277778	12.40741
0.0748	8.682487	9.346257	9.759358289	10.02005
0.1453	4.73159	5.056779	5.247763248	5.368204
0.2175	3.16092	3.356322	3.517241379	3.650575
0.291	2.360825	2.560137	2.651202749	2.792096
0.362	1.906077	2.071823	2.154696133	2.237569
0.432	1.631944	1.747685	1.805555556	1.886574
0.501	1.44012	1.526946	1.576846307	1.636727
0.57	1.278947	1.345614	1.407894737	1.491228

Table-5: Hall resistivity at room temperature

A. Sample: $(Fe_{1-x}Mn_x)_{75}P_{15}C_{10}$

B. Sample Size:
Length: $l=1.2x10^{-2}$ m.
Width: $w= 8 \times 10^{-4}$ m
Thickness: $t= 25 \times 10^{-6}$ m

Magnetic Field, H (tesla)	ρ_H(Ohm-m)x 10^{-8}, x=0.00	ρ_H(Ohm-m)x 10^{-8}, x=0.10	ρ_H(Ohm-m)x 10^{-8}, x=0.20	ρ_H(Ohm-m)x 10^{-8}, x=0.30
0	0	0	0	0
0.025	0.5934	0.5852	0.48	0.6423
0.033	0.7753	0.85231	0.8563	0.8236
0.0413	0.9632	1.023	1.0234	1.023
0.054	1.147	1.235	1.2531	1.34
0.0748	1.2989	1.3982	1.46	1.53
0.1453	1.375	1.4695	1.54	1.58
0.2175	1.375	1.46	1.53	1.588
0.291	1.374	1.47	1.53	1.625
0.362	1.38	1.5	1.54	1.62
0.432	1.41	1.51	1.56	1.63
0.501	1.443	1.53	1.58	1.64
0.57	1.458	1.51	1.58	1.7

Table-6: Magnetoresistance (MR%) room temperature

Magnetic field, H (T)	MR%, x=0.00	MR%, x=0.10	MR%, x=0.20	MR%, x=0.30
0	0	0	0	0
0.0748	1.6	1.85	2.08	2.26
0.1453	3.14	3.6	3.82	4.12

0.2175	3.4	4.07	4.64	5.5
0.291	3.03	3.87	4.4	5.23
0.362	2.8	3.66	4.43	5.28
0.432	3	3.91	4.89	5.74
0.501	3.87	4.4	5.39	6.04
0.57	4.77	5.4	6.57	7.50

Table-7: Real permeability at room temperature

Frequency, f (MHz)	μ', x=0.00	μ', x=0.10	μ', x=0.20
0.0001	3.7692E+00	3.7589E+00	3.7471E+00
0.001	3.7924E+00	3.7823E+00	3.7623E+00
0.01	3.9860E+00	3.8624E+00	3.8423E+00
0.5	4.2756E+00	4.1846E+00	3.9061E+00
1	4.3855E+00	4.1842E+00	4.0864E+00
1.5	4.5540E+00	4.4421E+00	4.3548E+00
2	4.7314E+00	4.5213E+00	4.6652E+00
2.5	5.0110E+00	4.9875E+00	5.0681E+00
3	5.2923E+00	5.1245E+00	5.4707E+00
3.5	5.6620E+00	5.4423E+00	5.8990E+00
4	6.0421E+00	6.0123E+00	6.3200E+00
4.5	6.4953E+00	6.4231E+00	6.7461E+00
5	6.9639E+00	6.9452E+00	7.1317E+00
5.5	7.4898E+00	7.4237E+00	7.4908E+00
6	8.0338E+00	8.0133E+00	7.8250E+00
6.5	8.6155E+00	8.5214E+00	8.1315E+00
7	9.2444E+00	9.1245E+00	8.4603E+00
7.5	9.9146E+00	9.9012E+00	8.7810E+00
8	1.0594E+01	1.0486E+01	9.1229E+00
8.5	1.1320E+01	1.1223E+01	9.4746E+00
9	1.2044E+01	1.2033E+01	9.8142E+00
9.5	1.2818E+01	1.2786E+01	1.0174E+01
10.5	1.3542E+01	1.3496E+01	1.0499E+01
11	1.4320E+01	1.4223E+01	1.0875E+01
11.5	1.5037E+01	1.5031E+01	1.1217E+01
12	1.5763E+01	1.5722E+01	1.1567E+01
12.5	1.6464E+01	1.6412E+01	1.1917E+01
13	1.7119E+01	1.7093E+01	1.2243E+01
13.5	1.7745E+01	1.7682E+01	1.2610E+01

14	1.8333E+01	1.6324E+01	1.2957E+01
14.5	1.8893E+01	1.5540E+01	1.3301E+01
15	1.9424E+01	1.7300E+01	1.3643E+01
15.5	1.9910E+01	1.7325E+01	1.4088E+01
16	2.0423E+01	1.8255E+01	1.4431E+01
16.5	2.0878E+01	1.8865E+01	1.4783E+01
17	2.1263E+01	1.8992E+01	1.5117E+01
17.5	2.1702E+01	1.9215E+01	1.5457E+01
18	2.2086E+01	1.9992E+01	1.5779E+01
18.5	2.2486E+01	2.0021E+01	1.6148E+01
19	2.2854E+01	2.0123E+01	1.6450E+01
19.5	2.3251E+01	2.0230E+01	1.6739E+01
20	2.3607E+01	2.0324E+01	1.7088E+01
20.5	2.4021E+01	2.1235E+01	1.7432E+01
21	2.4348E+01	2.1569E+01	1.7741E+01
21.5	2.4713E+01	2.1896E+01	1.8065E+01
22	2.5142E+01	2.2456E+01	1.8384E+01
22.5	2.5486E+01	2.2568E+01	1.8676E+01
23	2.5886E+01	2.2790E+01	1.9019E+01
23.5	2.6289E+01	2.2897E+01	1.9312E+01
24	2.6721E+01	2.3421E+01	1.9662E+01
24.5	2.7055E+01	2.3965E+01	1.9941E+01
25	2.7465E+01	2.3996E+01	2.0228E+01
25.5	2.7880E+01	2.4880E+01	2.0546E+01
26	2.8327E+01	2.4365E+01	2.0828E+01
26.5	2.8704E+01	2.4854E+01	2.1158E+01
27	2.9148E+01	2.5012E+01	2.1444E+01
27.5	2.9607E+01	2.5214E+01	2.1743E+01
28	2.9974E+01	2.5865E+01	2.2035E+01
28.5	3.0427E+01	2.6324E+01	2.2369E+01
29	3.0875E+01	2.6356E+01	2.2646E+01
29.5	3.1347E+01	2.7365E+01	2.2923E+01
30	3.1768E+01	2.7986E+01	2.3212E+01
30.5	3.2221E+01	2.8000E+01	2.3509E+01
31	3.2712E+01	2.8366E+01	2.3886E+01
31.5	3.3170E+01	2.9569E+01	2.4123E+01
32	3.3603E+01	3.0236E+01	2.4387E+01
32.5	3.4085E+01	3.0759E+01	2.4708E+01
33	3.4503E+01	3.0986E+01	2.4934E+01
33.5	3.4977E+01	3.1217E+01	2.5278E+01

34	3.5413E+01	3.1786E+01	2.5539E+01
34.5	3.5906E+01	3.2569E+01	2.5851E+01
35	3.6362E+01	3.2749E+01	2.6133E+01
35.5	3.6832E+01	3.3215E+01	2.6415E+01
36	3.7320E+01	3.3990E+01	2.6744E+01
36.5	3.7790E+01	3.4256E+01	2.7071E+01
37	3.8248E+01	3.4990E+01	2.7376E+01
37.5	3.8691E+01	3.5265E+01	2.7631E+01
38	3.9183E+01	3.5968E+01	2.7955E+01
38.5	3.9641E+01	3.6321E+01	2.8298E+01
39	4.0152E+01	3.6456E+01	2.8573E+01
39.5	4.0641E+01	3.7123E+01	2.8958E+01
40	4.1135E+01	3.7956E+01	2.9253E+01
40.5	4.1538E+01	3.8032E+01	2.9586E+01
41	4.2059E+01	3.9012E+01	2.9844E+01
41.5	4.2481E+01	3.9587E+01	3.0258E+01
42	4.2989E+01	3.9876E+01	3.0498E+01
42.5	4.3393E+01	3.9987E+01	3.0896E+01
43	4.3883E+01	4.0256E+01	3.1121E+01
43.5	4.4350E+01	4.0959E+01	3.1465E+01
44	4.4832E+01	4.1256E+01	3.1850E+01
44.5	4.5241E+01	4.1986E+01	3.2117E+01
45	4.5648E+01	4.2365E+01	3.2477E+01
45.5	4.6136E+01	4.2896E+01	3.2799E+01
46	4.6649E+01	4.3996E+01	3.3149E+01
46.5	4.7094E+01	4.4569E+01	3.3452E+01
47	4.7554E+01	4.4996E+01	3.3810E+01
47.5	4.8014E+01	4.5263E+01	3.4158E+01
48	4.8461E+01	4.5367E+01	3.4468E+01
48.5	4.8895E+01	4.5996E+01	3.4807E+01
49	4.9372E+01	4.6356E+01	3.5229E+01
49.5	4.9788E+01	4.6896E+01	3.5495E+01
50	5.0252E+01	4.7023E+01	3.5856E+01
50.5	5.0728E+01	4.7698E+01	3.6224E+01
51	5.1175E+01	4.8563E+01	3.6605E+01
51.5	5.1628E+01	4.8965E+01	3.6997E+01
52	5.2108E+01	4.9365E+01	3.7370E+01
52.5	5.2527E+01	4.9965E+01	3.7737E+01
53	5.3013E+01	5.0123E+01	3.8093E+01
53.5	5.3412E+01	5.0698E+01	3.8443E+01

54	5.3817E+01	5.0965E+01	3.8868E+01
54.5	5.4377E+01	5.1236E+01	3.9282E+01
55	5.4789E+01	5.1896E+01	3.9611E+01
55.5	5.5232E+01	5.2169E+01	3.9953E+01
56	5.5659E+01	5.2869E+01	4.0351E+01
56.5	5.6069E+01	5.3245E+01	4.0756E+01
57	5.6585E+01	5.3965E+01	4.1012E+01
57.5	5.6977E+01	5.3996E+01	4.1443E+01
58	5.7401E+01	5.4365E+01	4.1839E+01
58.5	5.7849E+01	5.4896E+01	4.2111E+01
59	5.8290E+01	5.5360E+01	4.2612E+01
59.5	5.8826E+01	5.5756E+01	4.2989E+01
60	5.9234E+01	5.6698E+01	4.3358E+01
60.5	5.9626E+01	5.6897E+01	4.3708E+01
61	6.0208E+01	5.7365E+01	4.4154E+01
61.5	6.0584E+01	5.7897E+01	4.4548E+01
62	6.0897E+01	5.7996E+01	4.4947E+01
62.5	6.1420E+01	5.8424E+01	4.5316E+01
63	6.1891E+01	5.8896E+01	4.5638E+01
63.5	6.2313E+01	5.9456E+01	4.6035E+01
64	6.2607E+01	5.9896E+01	4.6423E+01
64.5	6.3091E+01	6.0456E+01	4.6753E+01
65	6.3551E+01	6.0896E+01	4.7202E+01
65.5	6.3934E+01	6.0996E+01	4.7601E+01
66	6.4358E+01	6.1123E+01	4.7988E+01
66.5	6.4908E+01	6.1756E+01	4.8411E+01
67	6.5318E+01	6.1965E+01	4.8833E+01
67.5	6.5690E+01	6.2586E+01	4.9202E+01
68	6.6089E+01	6.2965E+01	4.9646E+01
68.5	6.6469E+01	6.2990E+01	5.0012E+01
69	6.6896E+01	6.3123E+01	5.0447E+01
69.5	6.7273E+01	6.3568E+01	5.0659E+01
70	6.7713E+01	6.4235E+01	5.1108E+01
70.5	6.8093E+01	6.4897E+01	5.1427E+01
71	6.8487E+01	6.5324E+01	5.1824E+01
71.5	6.8882E+01	6.5897E+01	5.2248E+01
72	6.9280E+01	6.6356E+01	5.2589E+01
72.5	6.9664E+01	6.6896E+01	5.3001E+01
73	7.0091E+01	6.7024E+01	5.3406E+01
73.5	7.0536E+01	6.7986E+01	5.3811E+01

74	7.0991E+01	6.7993E+01	5.4255E+01
74.5	7.1298E+01	6.8000E+01	5.4446E+01
75	7.1618E+01	6.8658E+01	5.4967E+01
75.5	7.2090E+01	6.9356E+01	5.5229E+01
76	7.2396E+01	6.9896E+01	5.5551E+01
76.5	7.2719E+01	7.0213E+01	5.5943E+01
77	7.3130E+01	7.0236E+01	5.6309E+01
77.5	7.3577E+01	7.0965E+01	5.6616E+01
78	7.3869E+01	7.1236E+01	5.7061E+01
78.5	7.4142E+01	7.1866E+01	5.7238E+01
79	7.4641E+01	7.2356E+01	5.7713E+01
79.5	7.4884E+01	7.2896E+01	5.8069E+01
80	7.5389E+01	7.3265E+01	5.8390E+01
80.5	7.5629E+01	7.2963E+01	5.8860E+01
81	7.5944E+01	7.3456E+01	5.9154E+01
81.5	7.6306E+01	7.3966E+01	5.9431E+01
82	7.6669E+01	7.4369E+01	5.9839E+01
82.5	7.6914E+01	7.4986E+01	6.0153E+01
83	7.7275E+01	7.5360E+01	6.0427E+01
83.5	7.7673E+01	7.5896E+01	6.0924E+01
84	7.7878E+01	7.5996E+01	6.1232E+01
84.5	7.8319E+01	7.6123E+01	6.1442E+01
85	7.8566E+01	7.6456E+01	6.2005E+01
85.5	7.8875E+01	7.6896E+01	6.2221E+01
86	7.9210E+01	7.7856E+01	6.2439E+01
86.5	7.9492E+01	7.7965E+01	6.2871E+01
87	7.9760E+01	7.8023E+01	6.3130E+01
87.5	7.9965E+01	7.8658E+01	6.3315E+01
88	8.0344E+01	7.8996E+01	6.3682E+01
88.5	8.0567E+01	7.9123E+01	6.4048E+01
89	8.0825E+01	7.9563E+01	6.4236E+01
89.5	8.1170E+01	7.9963E+01	6.4602E+01
90	8.1371E+01	8.0236E+01	6.4829E+01
90.5	8.1582E+01	8.0456E+01	6.5095E+01
91	8.1715E+01	8.0596E+01	6.5458E+01
91.5	8.1984E+01	8.0896E+01	6.5577E+01
92	8.2260E+01	8.1023E+01	6.5826E+01
92.5	8.2543E+01	8.0563E+01	6.6103E+01
93	8.2767E+01	8.0968E+01	6.6391E+01
93.5	8.2895E+01	8.1236E+01	6.6571E+01

94	8.3158E+01	8.1768E+01	6.6919E+01
94.5	8.3348E+01	8.1996E+01	6.7081E+01
95	8.3638E+01	8.2042E+01	6.7313E+01
95.5	8.3687E+01	8.2365E+01	6.7583E+01
96	8.3887E+01	8.2896E+01	6.7621E+01
96.5	8.4189E+01	8.2996E+01	6.7829E+01
97	8.4133E+01	8.3236E+01	6.7984E+01
97.5	8.4419E+01	8.3568E+01	6.8321E+01
98	8.4439E+01	8.3966E+01	6.8556E+01
98.5	8.4640E+01	8.4012E+01	6.8752E+01
99	8.4827E+01	8.4366E+01	6.8876E+01
99.5	8.4889E+01	8.4568E+01	6.9188E+01
100	8.4967E+01	8.4786E+01	6.9211E+01

Table-8: Imaginary permeability at room temperature

Frequency, f (MHz)	μ'', x=0.00	μ'', x=0.10	μ'', x=0.20
0.0001	1.9747E+03	1.8192E+03	1.2746E+03
0.001	1.9650E+03	1.7972E+03	1.2563E+03
0.01	1.9422E+03	1.7861E+03	1.2346E+03
0.5	1908.24531	1777.68011	1198.07427
1	1877.63388	1753.86613	1187.74503
1.5	1869.15363	1745.56042	1182.8269
2	1862.35971	1732.71602	1179.41696
2.5	1857.12302	1723.06263	1173.00351
3	1853.51248	1712.39788	1166.74971
3.5	1848.32531	1695.50358	1160.16023
4	1844.68467	1681.79468	1154.11462
4.5	1837.9529	1670.94558	1147.90702
5	1834.53944	1655.44952	1142.46316
5.5	1828.91538	1647.0522	1136.60526
6	1824.75438	1642.725	1132.00702
6.5	1819.72739	1631.37302	1128.02339
7	1814.35672	1621.71692	1124.80877
7.5	1809.12974	1614.56348	1121.36316
8	1803.66588	1612.80591	1118.65789

8.5	1798.0593	1601.34825	1115.59123
9	1791.53916	1594.12288	1113.3655
9.5	1786.07627	1580.09372	1111.26608
10.5	1779.07751	1578.21353	1108.96608
11	1771.90303	1567.45066	1106.70526
11.5	1764.92952	1556.79291	1104.57368
12	1757.82203	1548.21587	1102.80643
12.5	1750.91064	1545.71005	1101.39006
13	1744.04489	1541.2647	1099.85848
13.5	1737.64708	1534.8697	1098.34444
14	1731.06773	1530.51373	1097.05556
14.5	1724.61652	1528.19961	1095.59591
15	1718.67792	1523.91548	1094.37661
15.5	1710.61901	1518.65757	1091.41871
16	1705.1464	1515.42472	1090.07953
16.5	1700.25339	1512.21389	1088.89825
17	1695.40503	1510.02399	1087.47719
17.5	1690.98579	1507.84855	1086.1076
18	1687.05099	1502.68898	1084.80994
18.5	1683.42394	1498.54175	1083.60643
19	1679.81923	1493.40619	1082.14971
19.5	1676.49703	1482.28103	1080.92807
20	1673.61559	1475.16501	1079.79825
20.5	1670.96521	1472.06132	1078.18655
21	1668.03813	1472.55605	1077.29942
21.5	1665.53435	1465.67641	1075.92924
22	1663.12667	1464.76512	1074.82632
22.5	1661.10636	1461.87016	1073.63099
23	1658.75209	1457.37036	1072.67076
23.5	1656.55606	1450.74516	1071.57953
24	1654.95321	1446.231	1070.80877
24.5	1652.85232	1442.012	1069.88538
25	1651.10675	1438.214	1069.15848
25.5	1649.58157	1434.352	1068.33626
26	1648.09134	1430.14	1067.50409
26.5	1645.81278	1426.11	1066.7
27	1644.61671	1421.18	1066.11111
27.5	1643.05658	1416.15	1065.11871
28	1641.29451	1413.07	1064.47661
28.5	1639.6703	1409.12	1063.71813

29	1638.1791	1407.2	1062.77135
29.5	1636.85488	1405.22	1062.21579
30	1635.66949	1401.174	1061.4117
30.5	1634.14528	1394.5	1060.7807
31	1632.6065	1391.92742	1060.07427
31.5	1630.93084	1383.24194	1059.46784
32	1629.14353	1376.46774	1058.90585
32.5	1628.09503	1375.16	1058.61637
33	1626.56499	1373.83871	1058.24678
33.5	1624.8369	1370.89516	1057.68304
34	1623.75636	1372.30242	1057.18772
34.5	1622.35641	1366.98387	1056.93626
35	1620.82249	1365.02823	1056.39766
35.5	1619.37789	1359.10081	1056.08187
36	1618.31482	1357.37097	1055.62982
36.5	1617.03138	1356.12097	1055.15965
37	1615.4994	1354.22984	1054.5848
37.5	1614.10625	1350.35484	1054.02924
38	1612.55776	1349.24194	1053.27719
38.5	1611.65974	1347.78629	1052.78012
39	1609.80836	1343.875	1052.16374
39.5	1608.66568	1338.875	1051.51637
40	1607.36088	1336.77823	1050.8655
40.5	1606.06578	1334.87903	1050.14912
41	1604.69011	1332.17742	1049.3117
41.5	1603.68141	1331.40323	1048.69006
42	1602.05817	1330.29032	1048.02982
42.5	1600.72424	1325.93548	1047.43567
43	1599.75341	1324.83065	1046.89064
43.5	1598.5321	1323.8871	1046.26023
44	1597.10594	1318.76613	1045.74152
44.5	1595.91375	1314.35887	1045.42749
45	1594.83418	1310.22581	1044.98363
45.5	1593.43909	1306.76613	1044.87895
46	1592.20322	1302.61694	1044.63275
46.5	1591.0751	1298.87097	1044.38012
47	1589.98097	1287.51613	1044.12865
47.5	1588.72956	1283.35887	1043.94503
48	1587.55	1282.34677	1043.59591
48.5	1586.39859	1279.81855	1043.55439

49	1585.52872	1276.16129	1043.41228
49.5	1583.98897	1272.82661	1043.34211
50	1583.09871	1268.22984	1043.44678
50.5	1581.82304	1266.40323	1043.14561
51	1580.86967	1262.14	1042.86725
51.5	1579.37944	1261.452	1042.63275
52	1578.52122	1256.81452	1042.23333
52.5	1577.3368	1256.10484	1041.95263
53	1576.25626	1253.40726	1041.60058
53.5	1575.19028	1245.70968	1041.11053
54	1574.434	1241.96371	1040.80058
54.5	1573.11075	1234.58871	1040.11111
55	1571.94575	1231.75	1039.47953
55.5	1571.20889	1228.39234	1038.91637
56	1570.05262	1227.65887	1038.08421
56.5	1568.93422	1222.48589	1037.33333
57	1567.73038	1220.64637	1036.62515
57.5	1567.00711	1214.80403	1035.90877
58	1565.89647	1211.65565	1035.07135
58.5	1564.60623	1209.13024	1034.60234
59	1563.36841	1207.94274	1033.9076
59.5	1562.42088	1205.24153	1033.58363
60	1561.60829	1203.50161	1032.84971
60.5	1560.69958	1201.78387	1032.37427
61	1559.63943	1199.03871	1032
61.5	1558.88315	1197.1	1031.54386
62	1557.70747	1196.21008	1031.40468
62.5	1556.62887	1195.69153	1031.57427
63	1555.93181	1194.13468	1031.46374
63.5	1554.51148	1193.16452	1031.33158
64	1553.44161	1191.48185	1031.12047
64.5	1552.31447	1189.57379	1031.00702
65	1551.78148	1188.77339	1030.98246
65.5	1550.40484	1187.54234	1030.77719
66	1549.24275	1185.30444	1030.57018
66.5	1548.63792	1182.74153	1030.33333
67	1547.77873	1181.42702	1029.9848
67.5	1546.43121	1180.59718	1029.5269
68	1545.91569	1179.06653	1029.3076
68.5	1544.76234	1177.64556	1028.69649

69	1544.04975	1175.81411	1028.29006
69.5	1542.83426	1173.00161	1027.72456
70	1542.20904	1172.37823	1027.05673
70.5	1541.23238	1170.08306	1026.5614
71	1540.07708	1171.85766	1025.97836
71.5	1539.03052	1168.08387	1025.37251
72	1538.24997	1166.29839	1024.82632
72.5	1536.98594	1165.56653	1024.27193
73	1536.09957	1165.93911	1023.50409
73.5	1535.2365	1163.50202	1022.86023
74	1534.19867	1162.47903	1022.12339
74.5	1533.11813	1161.01774	1021.42398
75	1532.45602	1159.91935	1020.83216
75.5	1531.52305	1157.05927	1019.99415
76	1530.38814	1155.32984	1019.58363
76.5	1529.44255	1154.84073	1018.95439
77	1528.77946	1152.72379	1018.37485
77.5	1527.73679	1152.87581	1017.99883
78	1526.74071	1150.18468	1017.27836
78.5	1525.74172	1149.62097	1016.98538
79	1524.74564	1147.87298	1016.77135
79.5	1523.58064	1143.34758	1016.27953
80	1522.55543	1142.6371	1016.02573
80.5	1521.73799	1142.78508	1016.00643
81	1520.99627	1139.21855	1015.50292
81.5	1520.02738	1137.89556	1015.55673
82	1519.26624	1135.8254	1015.35146
82.5	1518.30997	1133.71653	1014.72924
83	1517.16244	1132.92379	1014.78889
83.5	1516.51198	1130.68105	1014.21053
84	1515.76832	1128.0879	1013.4462
84.5	1514.68681	1126.31008	1013.10409
85	1513.66161	1126.12903	1012.25205
85.5	1512.82572	1124.46855	1011.73158
86	1512.07623	1123.62863	1011.48421
86.5	1511.1384	1121.74839	1010.65965
87	1509.93845	1119.05685	1010.12222
87.5	1509.25983	1117.00484	1009.72047
88	1508.44822	1114.49597	1009
88.5	1507.5599	1112.08589	1008.52807

89	1506.72789	1110.52782	1008.11462
89.5	1505.9056	1109.71048	1007.3614
90	1505.1066	1107.99315	1007.00819
90.5	1503.95907	1105.28306	1006.5462
91	1503.18046	1104.43992	1006.01462
91.5	1502.43874	1102.47339	1005.82398
92	1501.52324	1100.39718	1005.22865
92.5	1500.62036	1099.8004	1004.48889
93	1499.82719	1097.93548	1004.34503
93.5	1498.97383	1096.11935	1003.63684
94	1497.93891	1094.76411	1003.14269
94.5	1497.16322	1092.35565	1003.06023
95	1496.25646	1091.39395	1002.5117
95.5	1495.68755	1089.66048	1002.23099
96	1494.76331	1088.00968	1001.93977
96.5	1493.89053	1087.325	1001.64737
97	1493.30123	1085.93911	1001.35556
97.5	1492.41583	1084.94073	1001.53801
98	1491.46635	1082.97863	1001.13099
98.5	1490.80327	1080.99516	1001.04854
99	1490.01495	1078.0125	1001.08304
99.5	1489.0179	1079.55806	1000.80234
100	1488.2888	1078.01008	1001.01053

Table- 9: Magnetization measurement

Magnetic field, H	magnetization, M (emu/g), x=0.00	magnetization, M (emu/g), x=0.10	magnetization, M(emu/g), x=0.20	magnetization, M (emu/g), x=0.30
0	0	0	0	0
27	10	5.5	3.2	2.3
77	39.1	16	10.3	6.23
167	76.8	32	22.2	12.8
237	100	44.2	32	17.3
277	110	53	38.1	21.284
347	125.6056	64	48.6	23.924
437	139.5634	76.9	60	27.5
467	142.8	80.9	65	28.2
547	147.5	88.3	71.4	29.81
617	150.2817	95.1	76.3	30.36
697	152.2817	102.5	80	30.99
767	153.5211	108	82.5	31.53

827	155.5211	111.2	83.2	31.98
930	155.5211	113.7	83.2	32.24
1000	155.5211	113.8646	83.2	32.24
1070	155.5211	113.8646	83.2	32.24
1141	155.5211	113.8646	83.2	32.24
1212	155.5211	113.8646	83.2	32.24
1284	155.5211	113.8646	83.2	32.24
1360	155.5211	113.8646	83.2	32.24
1426	155.5211	113.8646	83.2	32.24
1498	155.5211	113.8646	83.2	32.24
1570	155.5211	113.8646	83.2	32.24
1663	155.5211	113.8646	83.2	32.24
1719	155.5211	113.8646	83.2	32.24
1792	155.5211	113.8646	83.2	32.24
1861	155.5211	113.8646	83.2	32.24
1934	155.5211	113.8646	83.2	32.24
2007	155.5211	113.8646	83.2	32.24
2082	155.5211	113.8646	83.4	32.24
2153	155.5211	113.8646	83.2	32.24
2277	155.5211	113.8646	83.2	32.24
2347	155.5211	113.8646	83.2	32.24
2417	155.5211	113.8646	83.2	32.24
2477	155.5211	113.8646	83.2	32.24
2547	155.5211	113.8646	83.2	32.24
2617	155.5211	113.8646	83.2	32.24
2687	155.5211	113.8646	83.2	32.24
2747	155.5211	113.8646	83.2	32.24
2817	155.5211	113.8646	83.2	32.24

Table-10: Data for Saturation Magnetization

Samples	Saturation Magnetization , Ms (emu/g	Bohr Magneton per formula unit
x=0.00	155	1.33
x=0.10	114	0.97
x=0.20	83	0.71
x=0.30	32	0.23

Table-11: **DTA peak values of the different samples**

Samples	temperature (°C)
x=0.0	418
x=0.10	436
x=0.20	439
x=0.30	472